MAGYAR ÁLLAMI
EÖTVÖS LORÁND
GEOFIZIKAI INTÉZET

EÖTVÖS LORÁND
GEOPHYSICAL INSTITUTE
OF HUNGARY

GEOFIZIKAI KÖZLEMÉNYEK

GEOPHYSICAL TRANSACTIONS

ВЕНГЕРСКИЙ
ГЕОФИЗИЧЕСКИЙ
ИНСТИТУТ
ИМ Л. ЭТВЕША

ГЕОФИЗИЧЕСКИЙ
БЮЛЛЕТЕНЬ

CONTENTS

VOL. 32. NO. 1. MARCH 1986 (ISSN 0016–7177)

BUDAPEST

TARTALOMJEGYZÉK

СОДЕРЖАНИЕ

GEOPHYSICAL TRANSACTIONS 1986
Vol. 32. No. 1. pp. 3–29

PREDICTION OF OIL AND GAS RESERVOIRS OF COMPLEX STRUCTURE BY THE COMBINED USE OF SEISMIC AND BOREHOLE DATA

N. A. SAVOST'YANOV*, G. N. GOGONENKOV** and S. S. EL'MANOVICH**

A method is presented for predicting hydrocarbon reservoirs of complex structure by combining data from exploratory boreholes with results of detailed seismic surveys. The methodological background of the joint interpretation of geological and geophysical data is provided by concepts from seismic stratigraphy. A case history is presented from one of the productive areas of western Siberia, where the method was successfully applied.

Keywords: seismic survey, detail survey, seismic stratigraphy, seismic interpretation, pay zone, oil and gas reservoirs, well logs

1. Introduction

Nowadays, it is a frequently occurring problem in the oil industry that the CH reserves are distributed in reservoirs which have a highly intricate spatial pattern and an inhomogeneous interior structure. Conventional exploration methods, estimates of reserves and the planning of production from such reservoirs are, as a rule, not too efficient if based on a network of exploratory drillings. The structural models of the reservoir will not correspond to reality and a substantial part of the wells would produce less than the calculated inflow. Problems of this kind most frequently occur in cases where the reservoirs are distributed in terrestrial deposits, in small deltas, or on paleoslopes where the regimes of sedimentation are strongly differentiated. Borrowing well-known terms from communications theory, we can state that for an economically reasonable density of the exploratory drillings we cannot sample the physical properties of the layers at such a rate which would satisfy the Nyquist criterion. Consequently, the reconstructed function will be burdened with serious errors.

The optimal solution to this problem seems to be the joint interpretation of the data from exploratory holes with the results of detailed seismic surveys. Rapid progress in the last 20 years, both in field technology and data processing, has resulted in a continual increase in the accuracy and detail of the mapping

* Central Office of Well Logging and Field Geophysics of the Ministry of Oil Industry, 113816 Moscow, nab. M. Thorez d. 26/1, USSR
** Central Geophysical Expedition of the Ministry of Oil Industry, 123298 Moscow, ul. Narodnogo Opolcheniya, d. 40, korp. 3, USSR
Manuscript received: 12 June, 1985

of geological bodies. Even though the vertical resolving power of the seismic method—today and in the conceivable future—lags behind that of well logs, still, in many cases the seismic data fairly well approximate the production characteristics of pay zones. On the other hand, the horizontal resolution of state-of-the-art seismic prospecting significantly exceeds that of boreholes.

The aim of the present work is to lay the methodological foundations of a complex interpretation technique for studying reservoirs of complex structure. The applicability of the method will be proven in connection with a project in one of the productive areas of western Siberia, within the limits of the Krasnoleninsk arch.

The general structural build-up of the region was investigated by seismic methods more than 10 years ago. The regional oil-capacity of the Jurassic sandy–shaly formation overlying the basement was determined on the basis of a sporadic set of exploratory boreholes. However, only 30% of the production wells located on the basis of these data, produced the calculated inflow of oil. In view of this the drilling of further production wells was suspended and repeated exploration called for.

For this purpose a network of 24-fold CDP profiles was designed (*Fig. 1*). The materials obtained, together with the available well logs and general geological data, served as a basis for the integrated interpretation. A schematic representation of the steps of the interpretation of the geological–geophysical information is given in *Fig. 2*. The decisive feature of the method is the application of the principles of seismic stratigraphy in the interpretation process. In other words, we are looking for those sedimentary environments which may produce the given reflection pattern. The sequence of operations and analyses applied during the interpretation can easily be understood from the flow chart (Fig. 2). In the first step a mutual match is established between seismic and borehole data. This is achieved by means of synthetic seismograms and 2-dimensional modelling. If we succeed in unambiguously identifying the marker phases of the seismic sections with the geological boundaries, we can proceed to the second stage—to the integrated seismic stratigraphic analysis—with the aim of constructing the sedimentation models of the productive layers. After the construction of the model, when we have already formed a general idea of the possible types of reservoirs, comes the next stage, viz. the quantitative estimation of the position and size of the prospective traps. The final step is the working out of recommendations for further geophysical work and drilling project.

2. Analysis of seismic sections

Before describing the above steps in detail, a few words are in order on the processing and visualization of the seismic data. An important task of processing (apart from the reduction of noise) is to transform the seismic traces to such a form where the wave characteristics have already disappeared and the shape and intensity of the signals reflect the distribution of the acoustic properties of

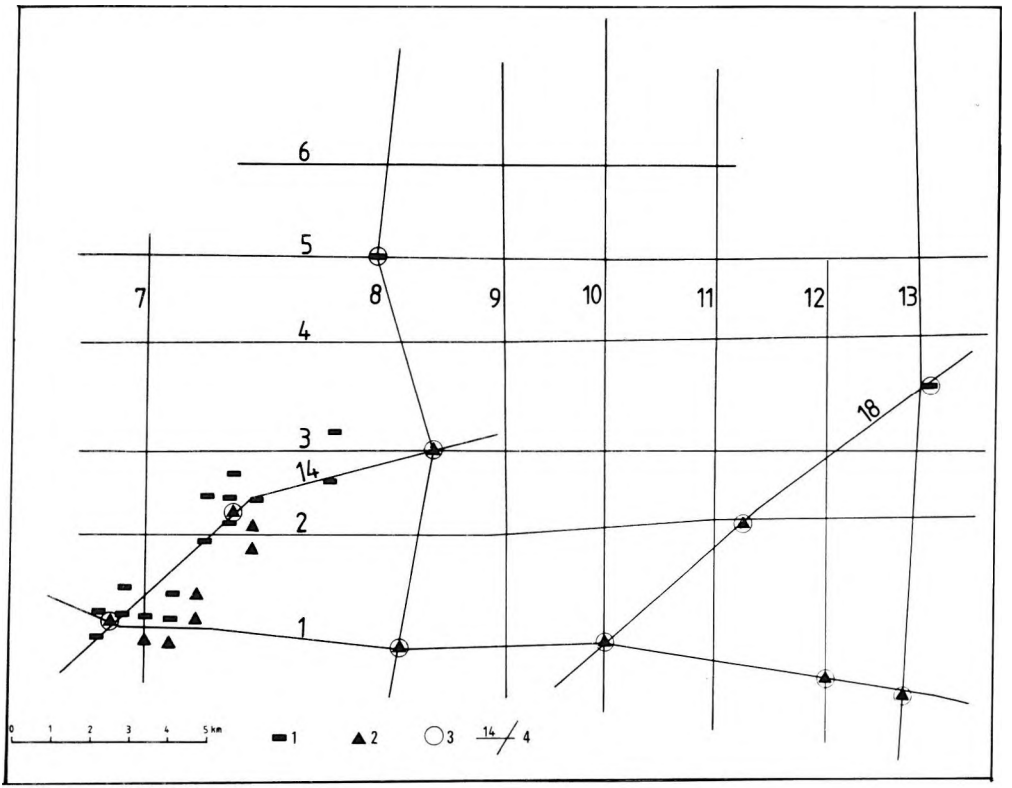

Fig. 1. Location map of the study area
1—dry wells; 2—productive wells; 3—exploratory boreholes; 4—seismic profiles

1. ábra. A kutatási terület helyszínrajza
1—meddő kutak; 2—produktív kutak; 3—kutató fúrások; 4—szeizmikus vonalak

Рис. 1. Схема расположения сейцмических профилей и скважин на Ем-Ёговской площади
1—непродуктивные скважины; 2—продуктивные скважины; 3—разведочные скважины; 4—сейсмические профили

the geological section. State-of-the-art data processing (including true amplitude recovery, wide-band deconvolution and migration) meets the above requirements.

Figure 3 shows a typical time section from the area. The productive interval, marked by an arrow, has a characteristic inhomogeneous structure. In *Fig. 4*, the well-log (SP) data are displayed in time scale, together with the seismic time section. The formation overlying the basement *(A)* is but weakly differentiated by the SP logs. For a more accurate stratigraphic identification

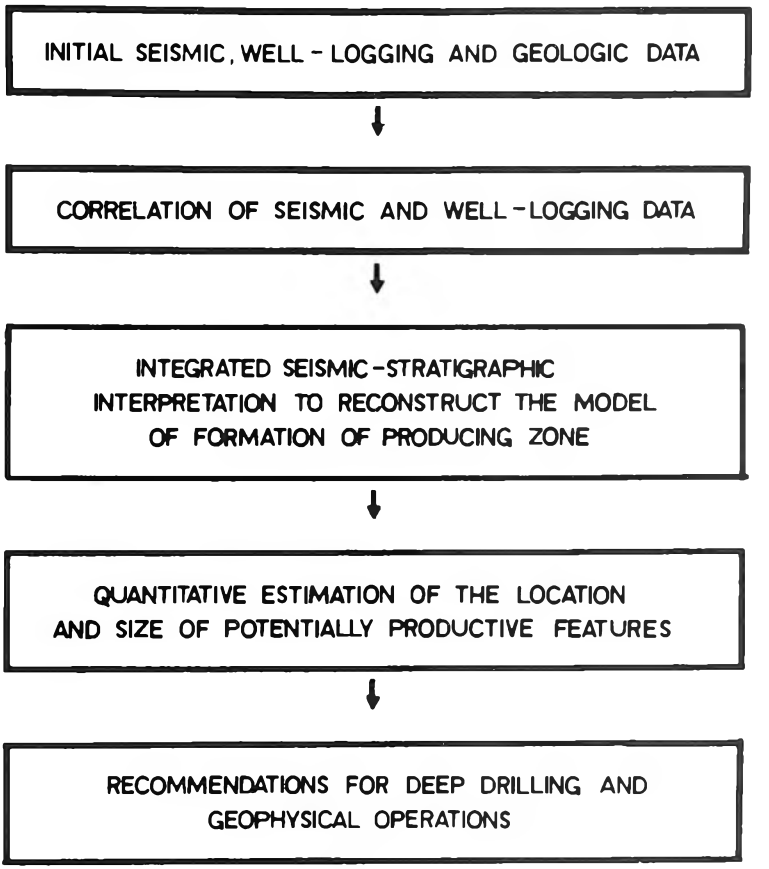

Fig. 2. Schematic flow-chart of the integrated interpretation of the geological–geophysical information. (For detailed block diagram see Gogonenkov et al. Geophys. Transactions 30, 2, p. 179)

2. ábra. A geológiai–geofizikai információ komplex értelmezésének vázlata (A részletes folyamatábrát lásd: Gogonenkov et al. Geofiz. Közl. 30, 2, p. 179)

Рис. 2. Схема комплексной интерпретации геолого-геофизической информации (Подробную блок-схему см. Гогоненков и др. Геофиз. Бюл. 30, 2, с. 179)

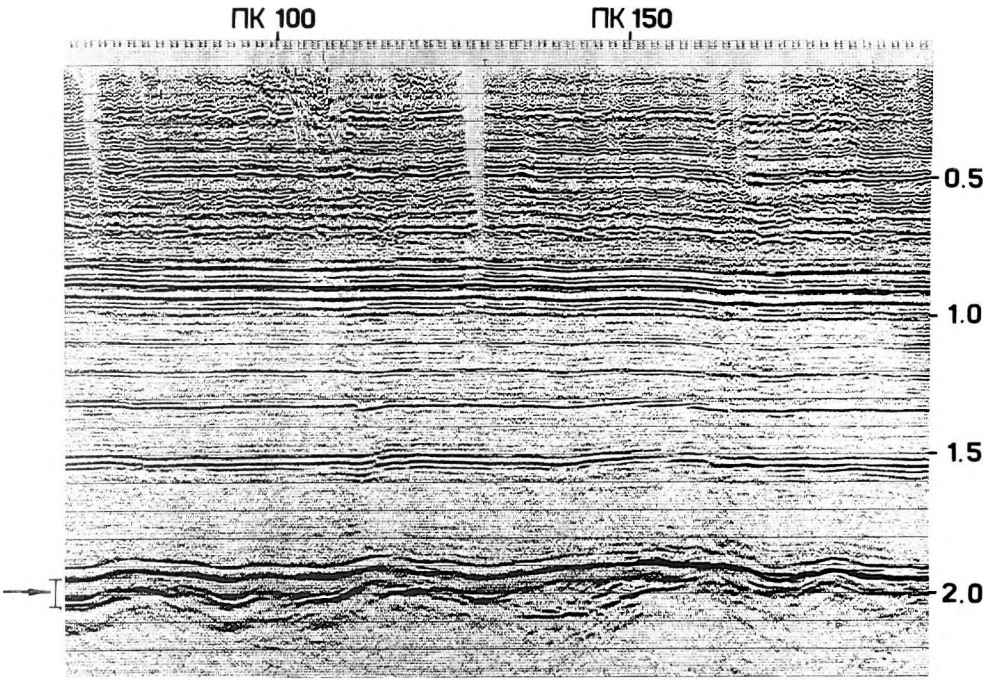

Fig. 3. Typical time section from the area of investigation

3. ábra. Időszelvény a kutatási területről

Рис. 3. Пример временного разреза площади исследований

of the phases of the seismic section the acoustic log was applied. *Figure 5* shows the input data utilized for the identification process. The central curve is the acoustic log; those above are, in turn, the spike trace, the synthetic traces and a series of seismic traces from the vicinity of the borehole. Below the acoustic log we see its filtered version in the characteristic frequency band of the seismic signals, and pseudoacoustic curves derived from the seismic traces by means of the familiar transformation.

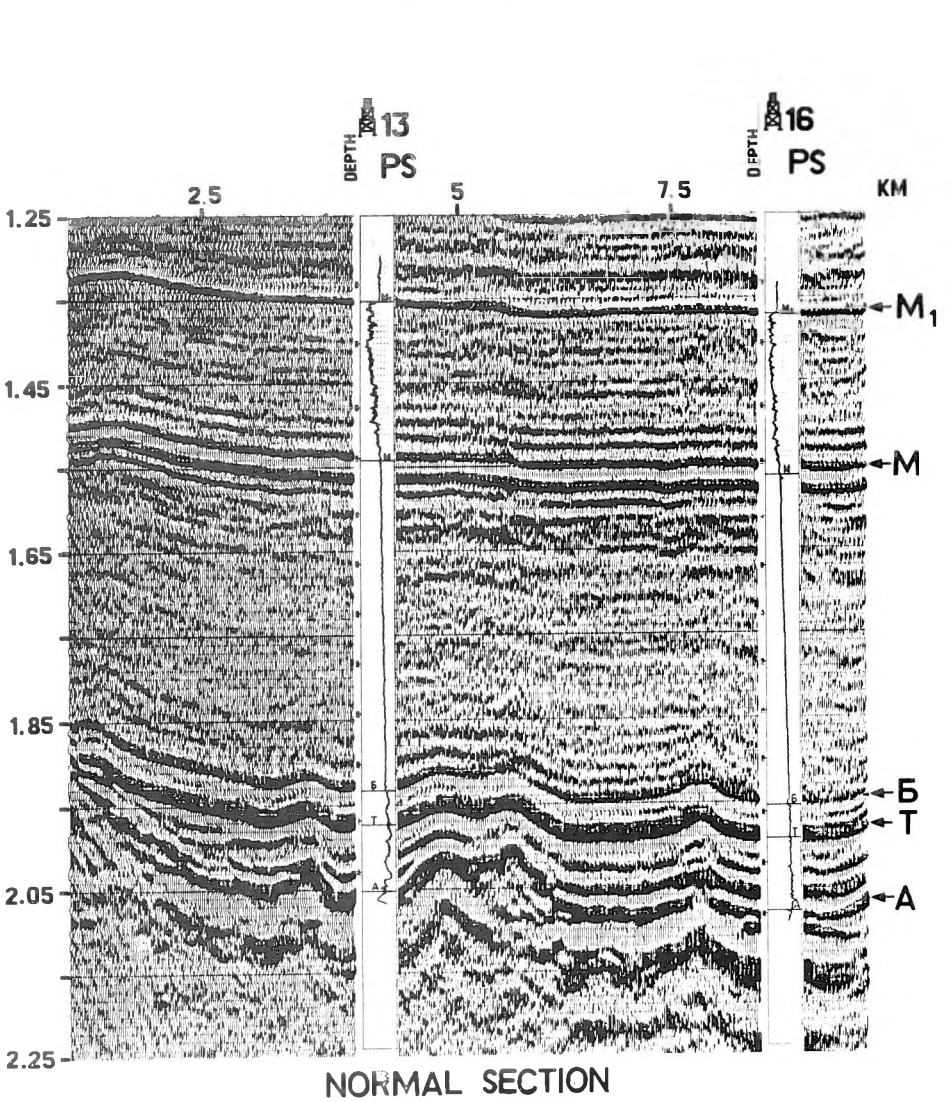

Fig. 4. Joint visualization of seismic- and well-log data

4. ábra. A karotázs- és a szeizmikus információk együttes ábrázolása

Рис. 4. Пример комплексирования промыслово-геофизической и сейсмической информации

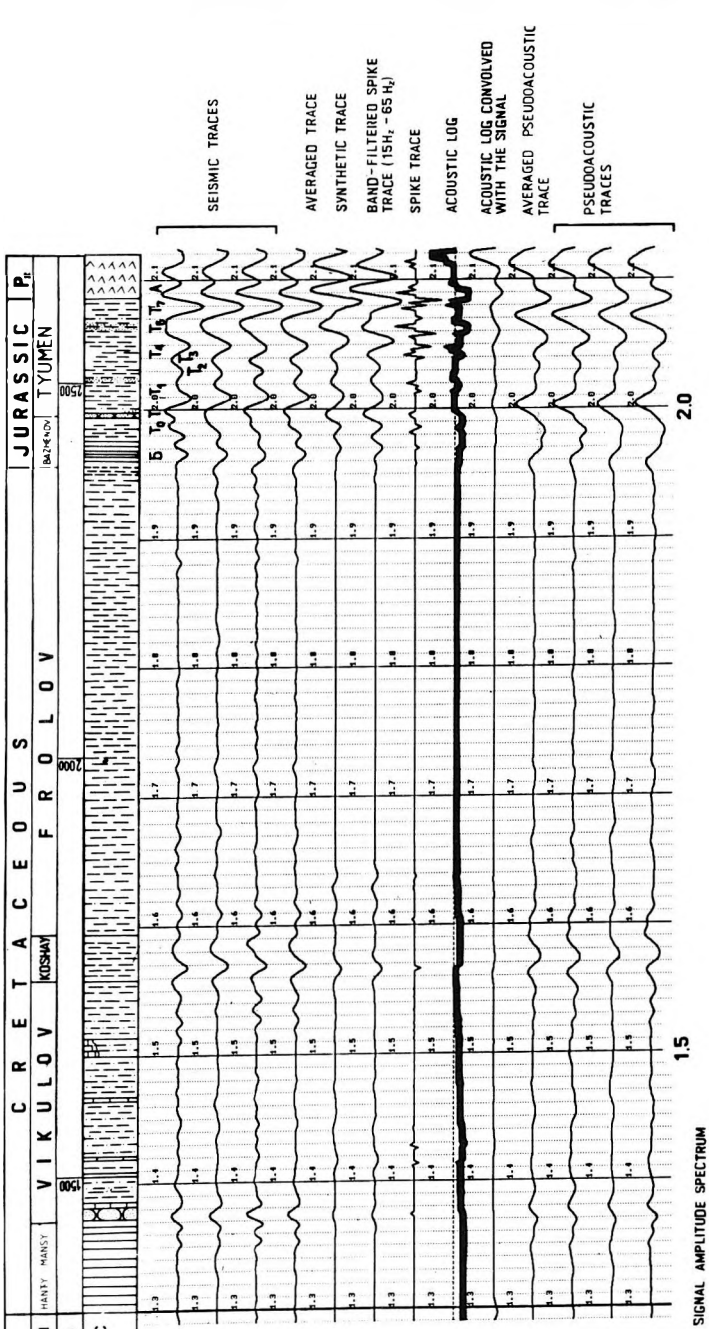

Fig. 5. Input material, used for stratigraphic correlation

5. ábra. Összesített adatok sztratigráfiai azonosításhoz

Рис. 5. Сводные данные, используемые для стратиграфической привязки

For further improvement of the match between seismic records and the geological section, the different phases of the seismic signals were identified with the particular geological bodies and their clusters by making use of so-called seismic lithofacies sections *(Fig. 6)*. A seismic lithofacies section is a joint display of a selected interval of the seismic time section shown in both polarities, and of the available borehole data. The use of such a seismic section renders possible a much more accurate correlation between the boreholes, that is, the model obtained is completely in conformity with all the available information. Before describing the next step, it should be noted that the conventional ways of displaying seismic time sections are inadequate as a means of analysing the behaviour of each phase of the seismic signals. In order to have a maximally compact representation of all information in a single black-and-white section, we developed a new technique, termed dual polarity section. In *Fig. 7* we show a detail of one of the sections in both polarities and, below, with the new technique. Evidently, the direct and inverse polarities, respectively, carry independent information on the geological build-up; this new kind of display preserves the information of the original polarities of the half-periods.

3. Setting up the geological model

In order to study conveniently the construction of the perspective formation we prepared a spatial model of the seismic facies (the fence diagram of *Fig. 8*). To facilitate its study a part of the system, the latitudinal profiles are presented in *Fig. 9*. In *Fig. 10* the same sections are shown in the paleoplane, i.e. after applying proper vertical displacements to the traces which "strip off" the effects of post-Jurassic tectonic movements. The section, just above the basement can be divided into *(i)* a lower part, characterized by a dynamically heterogeneous wave-field and—according to core-sample analyses—consisting of continental deposits; *(ii)* an upper part, judging by the much more persistent wave pattern and by borehole data, consisting of rather uniform marine deposits. The boundary between the layers of different genesis goes along reflection T, confined to basal sandstones created during the transgression of the sea. The seismic character of reflection T and of the overlying phases indicate that by the time of transgression the depositional surface had already been practically completely levelled by continental materials. This is why we decided to carry out the paleoreconstruction with respect to horizon T. After paleoreconstruction the resulting sections can be used to reconstruct the paleogeographical and paleotectonical conditions of the sedimentary basin.

In the early Jurrassic, the territory was a land of sharply differentiated topography. The chain of hills of a few hundred metres height, bordering the region on the south and west, were intensively eroded by water and the materials were redeposited on the slopes by temporary sand flows. On the deeper-lying parts tidal and lacustrine-marsh deposits were formed with intercalating coal seams. During the slow submergence of the whole territory the thickness of

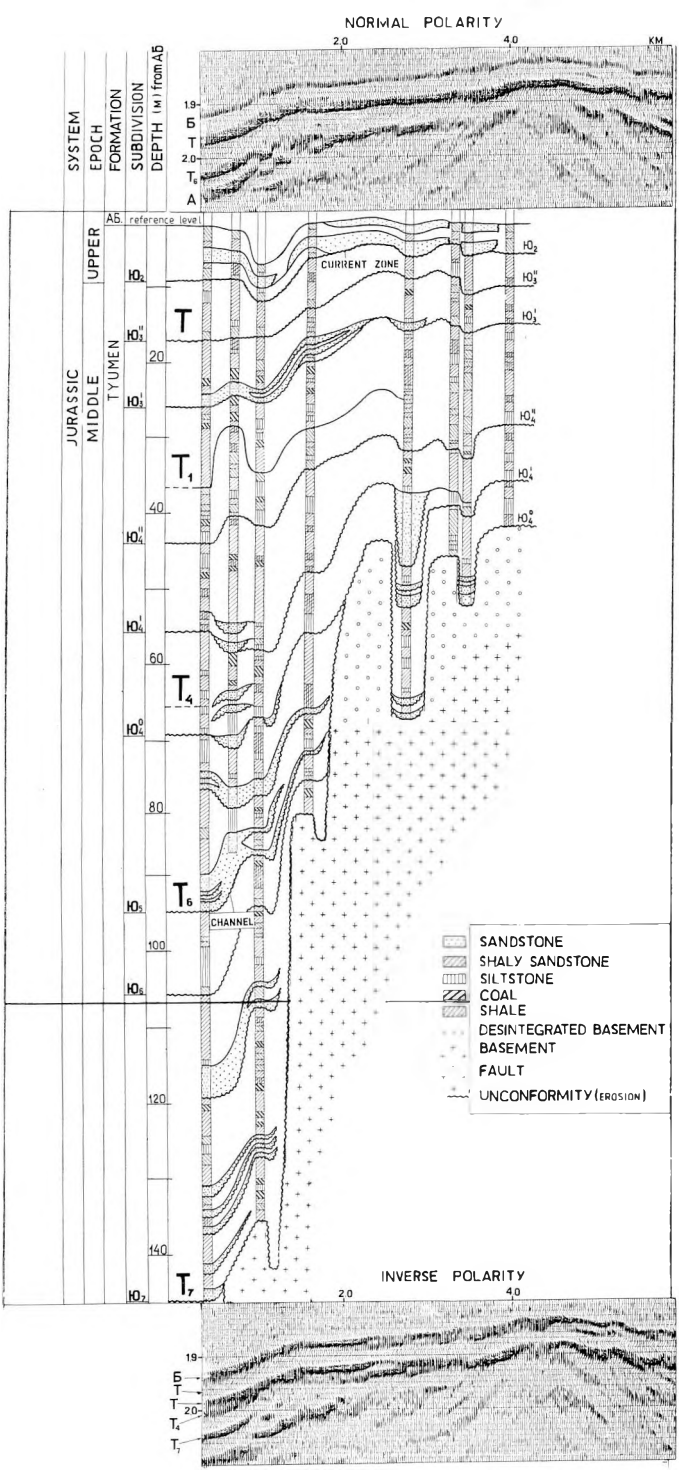

Fig. 6. Seismic lithofacies section for one of the seismic profiles

6. ábra. Szeizmolitofácies szelvény a kutatási terület egyik szeizmikus vonala mentén

Рис. 6. Сейсмолитофациальный разрез по одному из профилей площади исследований

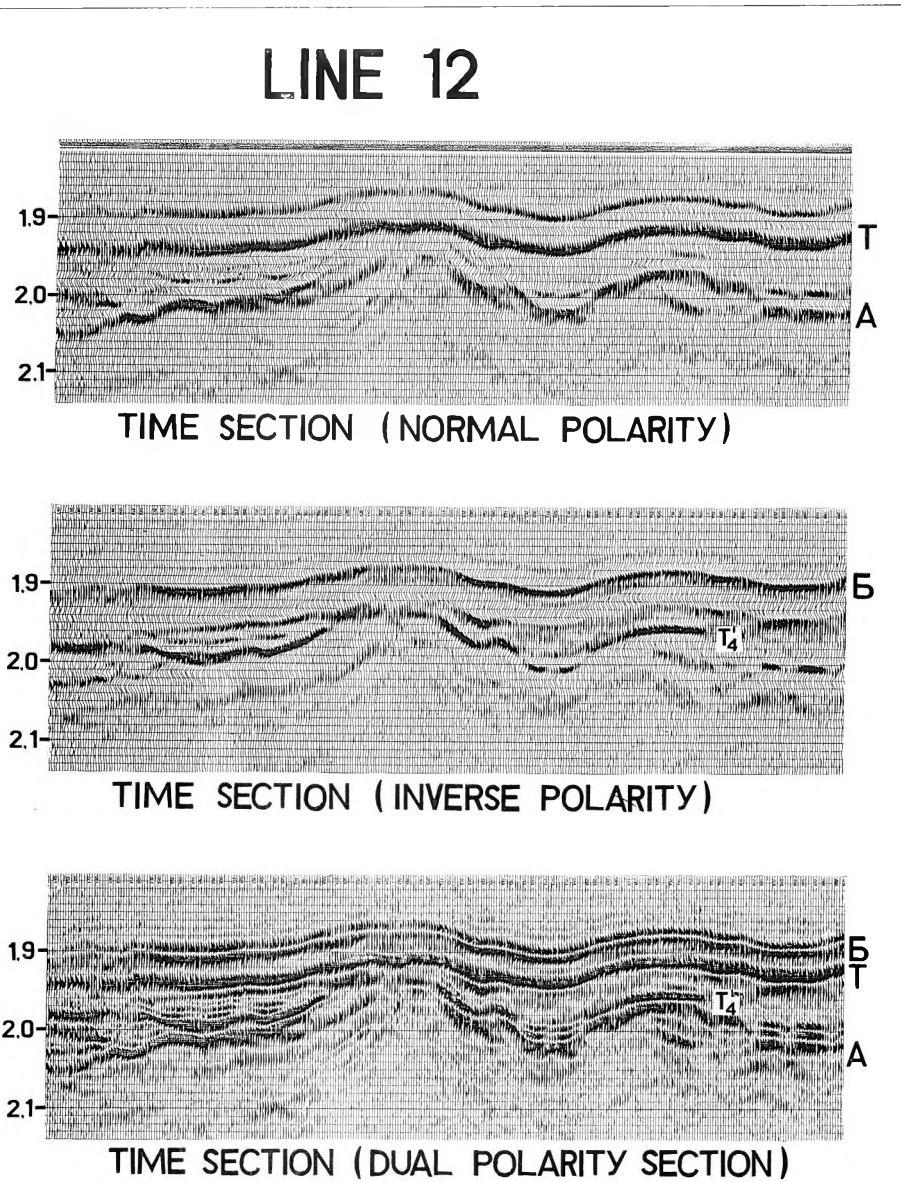

Fig. 7. Comparison of the different ways of visualizing time sections

7. ábra. Az időszelvények különböző megjelenítési módjainak összehasonlítása

Рис. 7. Сопоставление различных способов визуализации временных разрезов

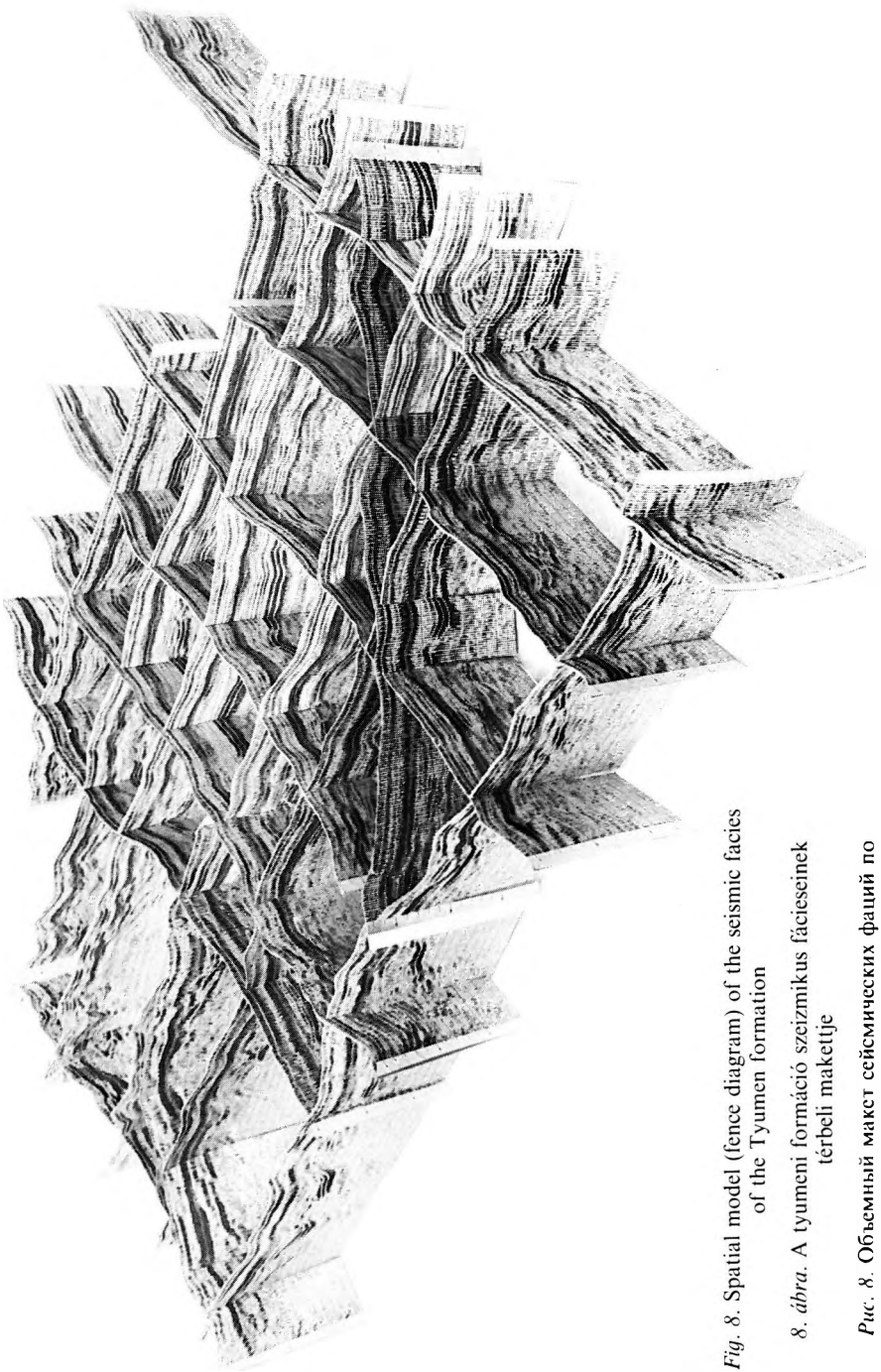

Fig. 8. Spatial model (fence diagram) of the seismic facies of the Tyumen formation

8. ábra. A tyumeni formáció szeizmikus fácieseinek térbeli makettje

Рис. 8. Объемный макет сейсмических фаций по интервалу тюменской свиты

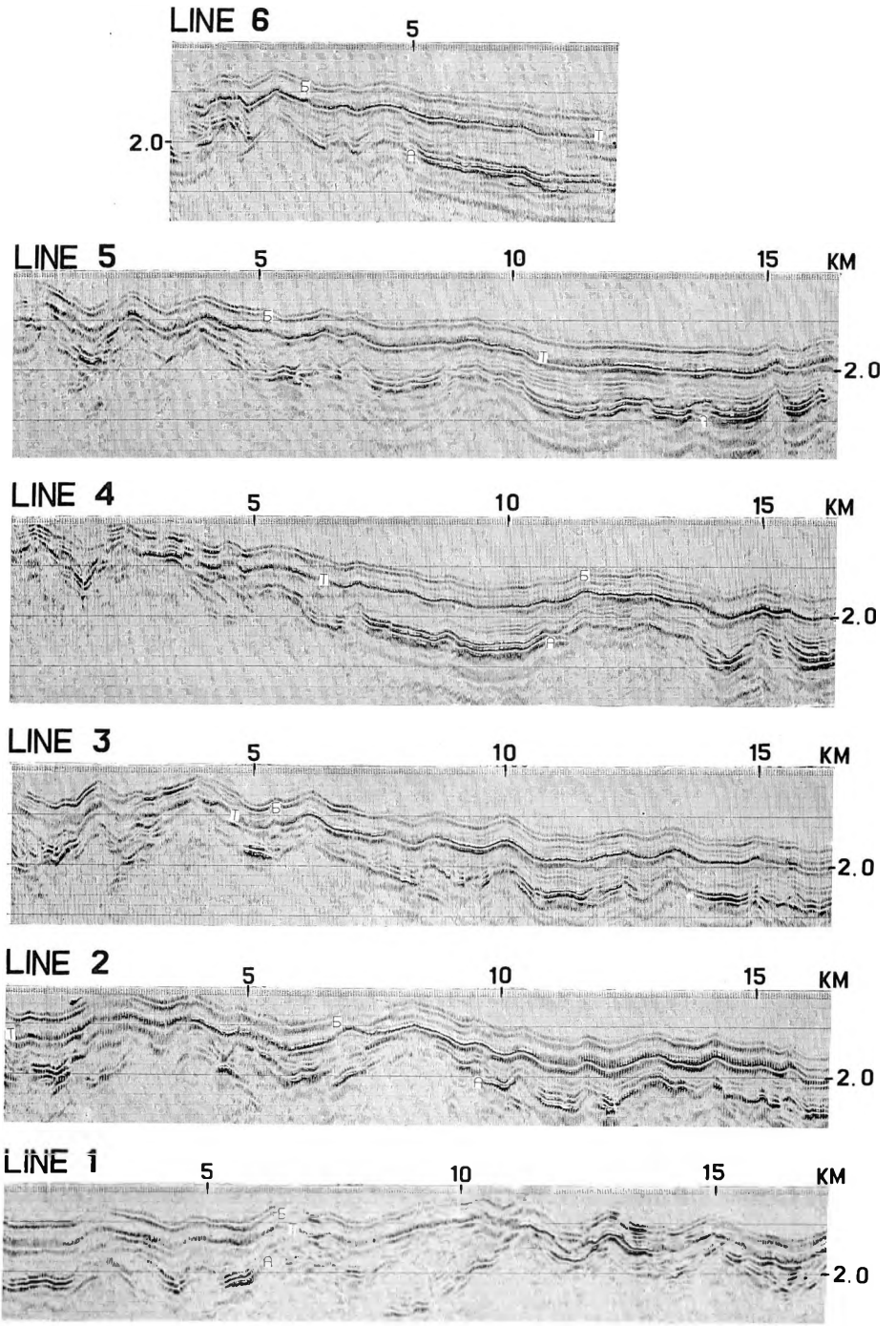
LINE 6
5
2.0
LINE 5
5
10
15
KM
2.0
LINE 4
5
10
15
KM
2.0
LINE 3
5
10
15
KM
2.0
LINE 2
5
10
15
KM
2.0
LINE 1
5
10
15
KM
2.0

terrestrial sediments gradually increased, due to the erosion and redeposition of the material of the nearby elevations. The process was accompanied by weak folding and faulting. In the paleo-walleys, which can easily be reconstructed from the seismic data, a network of rivers was formed *(Fig. 11)*. At a given time instant, the general subsidence of the basin, or the rise of the sea level, led to the transgression of the sea, this brought into being the sandstone layer of the Tyumen formation underlying the marine sedimentary sequence. The thickness of the sand is strikingly variable. To the elevated parts of the paleorelief there belong bar-type sand bodies. The overlying layer is homogeneous shale, which acts as an impermeable barrier. The weak tectonic activity has continued and has led to the present relief of the sedimentary complex.

Based on an analysis of this sedimentation model, the following main types of potential reservoirs can be distinguished:

- disintegrated parts of the basement surface, on the elevated blocks, due to fractures and erosion,
- proluvial fans and the weathered zones developed on the slopes of the basement highs,
- alluvial deposits in the deepest parts of the basin,
- the subfacies of local bars and channels within the Tyumen formation.

4. Search for prospective objects

The distribution of the physical properties of the investigated intervals were estimated from interval velocity maps constructed from pseudoacoustic sections. These maps were of decisive importance in determining the prospective objects. The statistical correlation established between seismic-, and production parameters rendered it possible to delineate these prospective objects.

The joint analysis of the pseudoacoustic velocities and the yield of oil wells tapping the basement (seismic horizon *A*) has proved a qualitative trend of decreasing velocities—increasing amount of oil. The zones of interval velocities of less than or equal to 3900 m/s may prove to be the most prospective *(Fig. 12)*; assigning the velocity decrease to the disintegration of the basement. On the interval velocity map of horizon *A (Fig. 13)* the decreased velocity zone of NW–SE strike corresponds to the elevated belt of the basement, and thus it is the prospective object of oil exploration below the sedimentary cover.

Fig. 9. Illustration of the seismic facies of the Tyumen formation by W–E-oriented time sections

9. ábra. A tyumeni formáció szeizmikus fácieseinek szemléltetése a kutatási területen, Ny–K irányú szelvényekkel

Рис. 9. Сейсмические фации тюменской свиты площади исследований на профилях широтного простирания

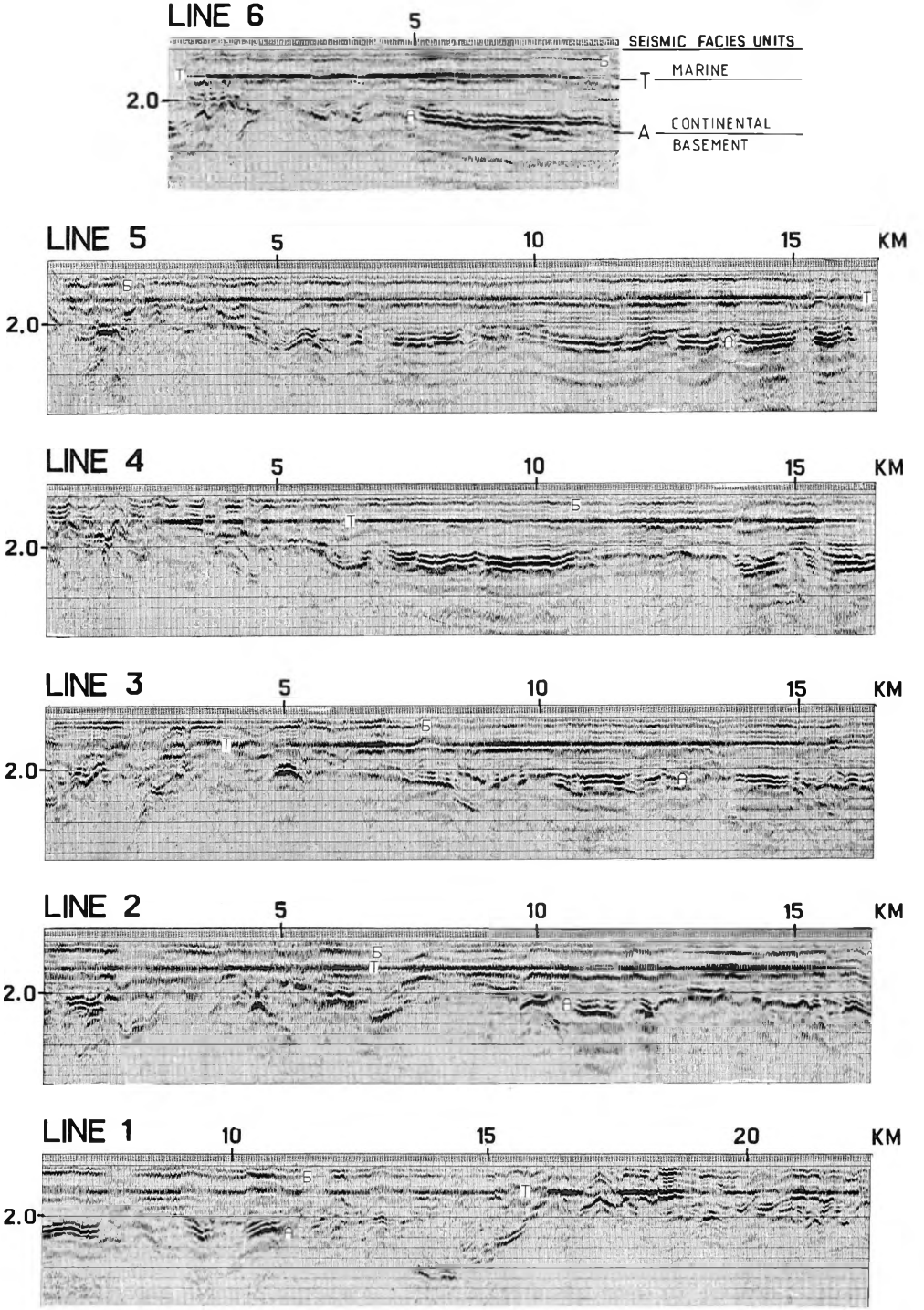
LINE 6
5
SEISMIC FACIES UNITS
T
MARINE
2.0
A
CONTINENTAL BASEMENT
LINE 5
5
10
15
KM
2.0
LINE 4
5
10
15
KM
2.0
LINE 3
5
10
15
KM
2.0
LINE 2
5
10
15
KM
2.0
LINE 1
10
15
20
KM
2.0

When analysing the reflections corresponding to the slope deposits we did not succeed in establishing a stable correlation between the seismic dynamic characteristics and the yield of oil from the given layer. Even so, although almost all drill-holes hitting the slope subfacies T'_4 are productive, a decrease of the pseudoacoustic interval velocity (3150–3500 m/s) towards the productive wells can be observed *(Fig. 14)*. Thus, the prospective objects along horizon T'_4 were selected if they met the criterion: $V_{pseudoacoustic} \leq 3400$ m/s.

The thicker zones of subfacies T_6 (seismic facies T_5) are regarded as channel fills, appearing with increased interval velocities (3950–4050 m/s) which, based on modelling studies, might be due to the increased sand content *(Fig. 15)*.

A detailed study of horizon T (sandstone formation at the base of the marine series) and the established correlation between seismic- and production parameters have proved that around the high-discharge wells characteristically high pseudoacoustic interval velocities are found. This general trend of the seismic interval velocities was also confirmed by modelling. It can be assumed that the zones of increased pseudoacoustic interval velocities *(Fig. 16)* signify parts of the formation with increased sand content, i.e. with more favourable reservoir properties.

On the basis of this study we concluded that the original concepts for the exploitation of the Em-Yogovsky oil field were not in agreement with the actual distribution of the reservoirs. As the productive bodies are situated in various scattered, non-anticlinal traps of complex structure and of different genesis, rather than in the originally supposed anticlinal structures *(Fig. 17)*.

The results of this work also show that our proposed new methodology of integrated interpretation of seismic and well-log data, based on seismic stratigraphic principles, has successfully solved the geological problems under the conditions of the structurally complex Tyumen formation within the Krasnoleninsk arch. On the basis of these results recommendations were given as to how the network of production wells should be changed. We suggested that the new drilling project should be carried out in two steps. First, boreholes should be located on selected points along the seismic profiles. If the production figures confirm the predicted conditions, the whole existing network of the production wells must be redesigned.

Fig. 10. Illustration of the seismic paleofacies of the Tyumen formation by W–E-oriented time sections

10. ábra. A tyumeni formáció paleoszeizmikus fácieseinek szemléltetése a kutatási területen, Ny–K irányú szelvényekkel

Рис. 10. Палеосейсмические фации тюменской свиты площади исследований на профилях широтного простирания

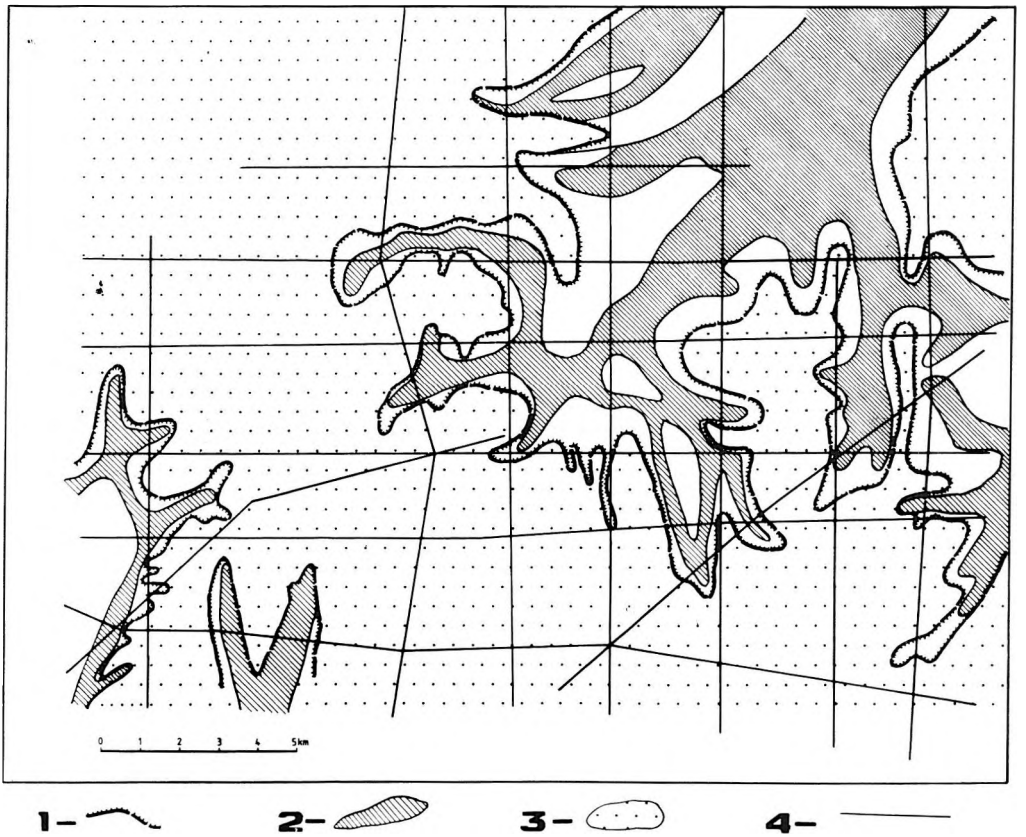

Fig. 11. Schematic paleogeographical map showing the development of the river network at the time of the Tyumen formation
1—sediment accumulation basin; 2—extension of the channel fill facies; 3—denudational highland (area of erosion); 4—seismic profile

11. ábra. A kutatási terület vázlatos ősföldrajzi térképe a tyumeni formáció képződési idejének folyórendszerével
1—üledékfelhalmozódási medence; 2—ősi folyómeder fácies elterjedésének területe; 3—denudációs fennsík (lehordási terület); 4—szeizmikus vonal

Рис. 11. Схематическая палеогеографическая карта развития речной сети в тюменское время
1—равнина низменная аккумулятивная; 2—области распространения древних русловых фаций; 3—равнина возвышения денудационная (область сноса); 4—сейсмические профили

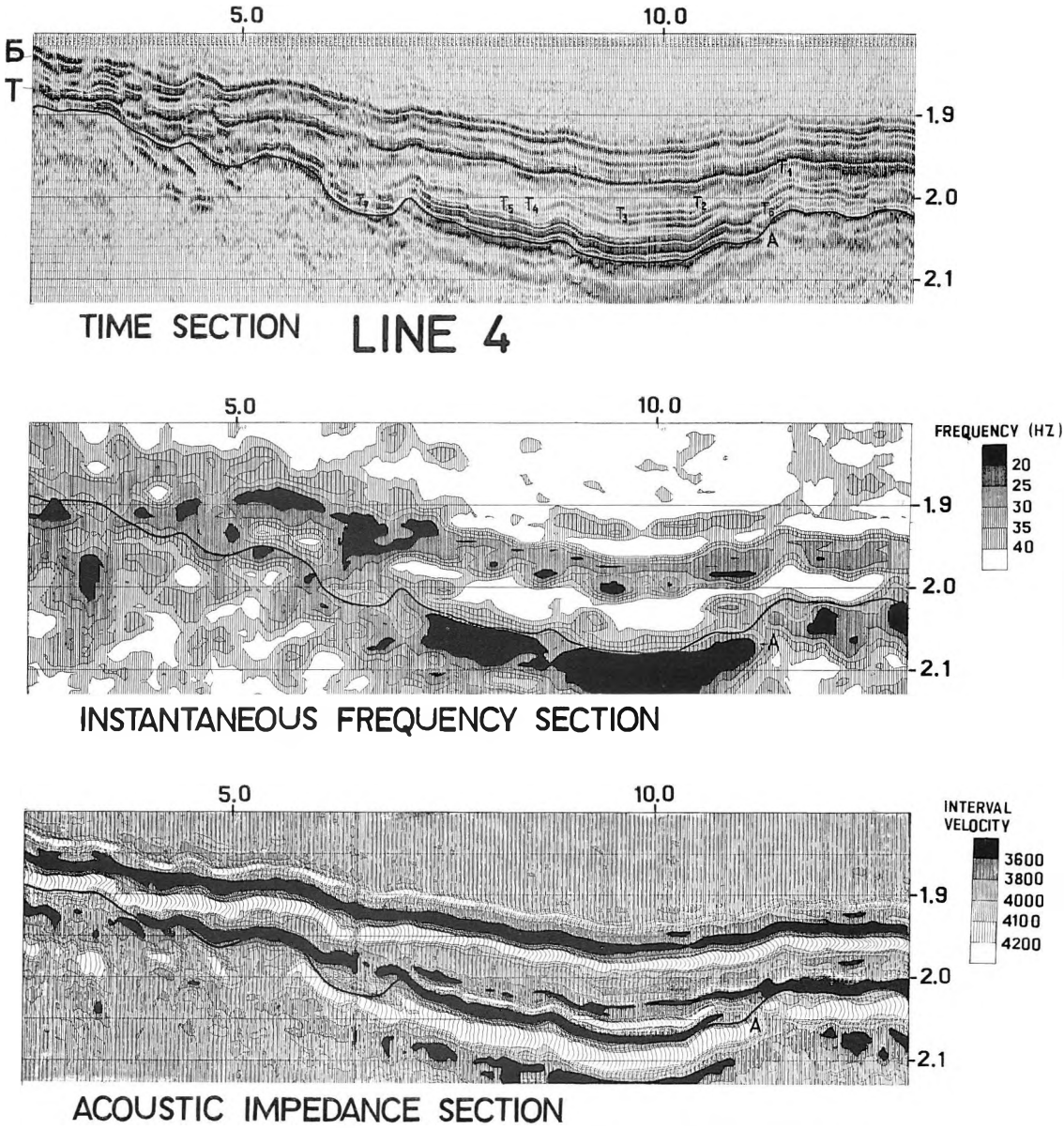

Fig. 12. Example for the character of wave pattern of seismic facies *A* in different tectonic zones

12. ábra. Példa az *A* jelű szeizmikus fácies hullámképi jellegére, különböző tektonikai zónákban

Рис. 12. Пример характера волновой картины сейсмической фации *A* в различных тектонических зонах

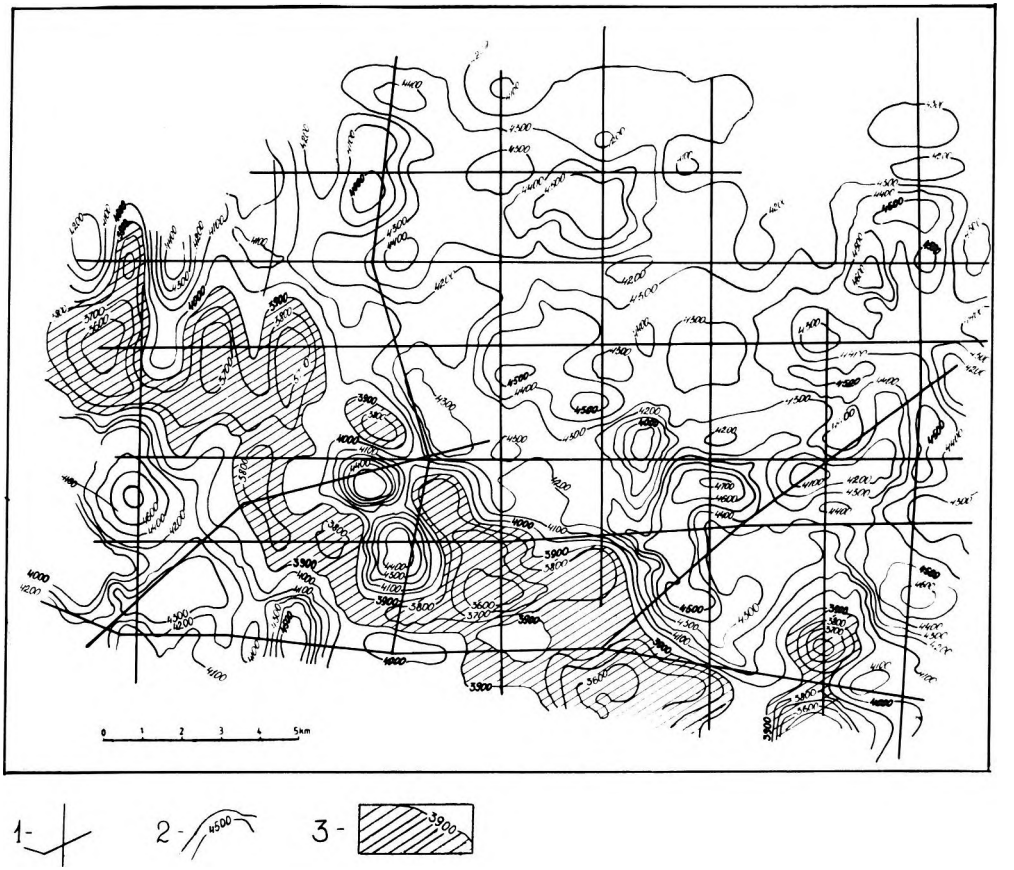

Fig. 13. Map of pseudoacoustic interval velocities along the surface of the basement (horizon *A*)
1—seismic profiles; 2—isolines of pseudoacoustic interval velocity; 3—interval velocity lower than 3900 m/s

13. ábra. Az aljzat felszínének (*A* szint) pszeudoakusztikus intervallumsebesség-térképe
1—szeizmikus vonalak; 2—a pszeudoakusztikus intervallumsebesség izovonalai;
3—az intervallumsebesség kisebb, mint 3900 m/s

Рис. 13. Карта интервальных скоростей ПАК по поверхности фундамента (горизонт *А*)
1—сейсмические профили; 2—изолинии псевдоакустической интервальной скорости;
3—интервальная скорость ниже 3900 м/с

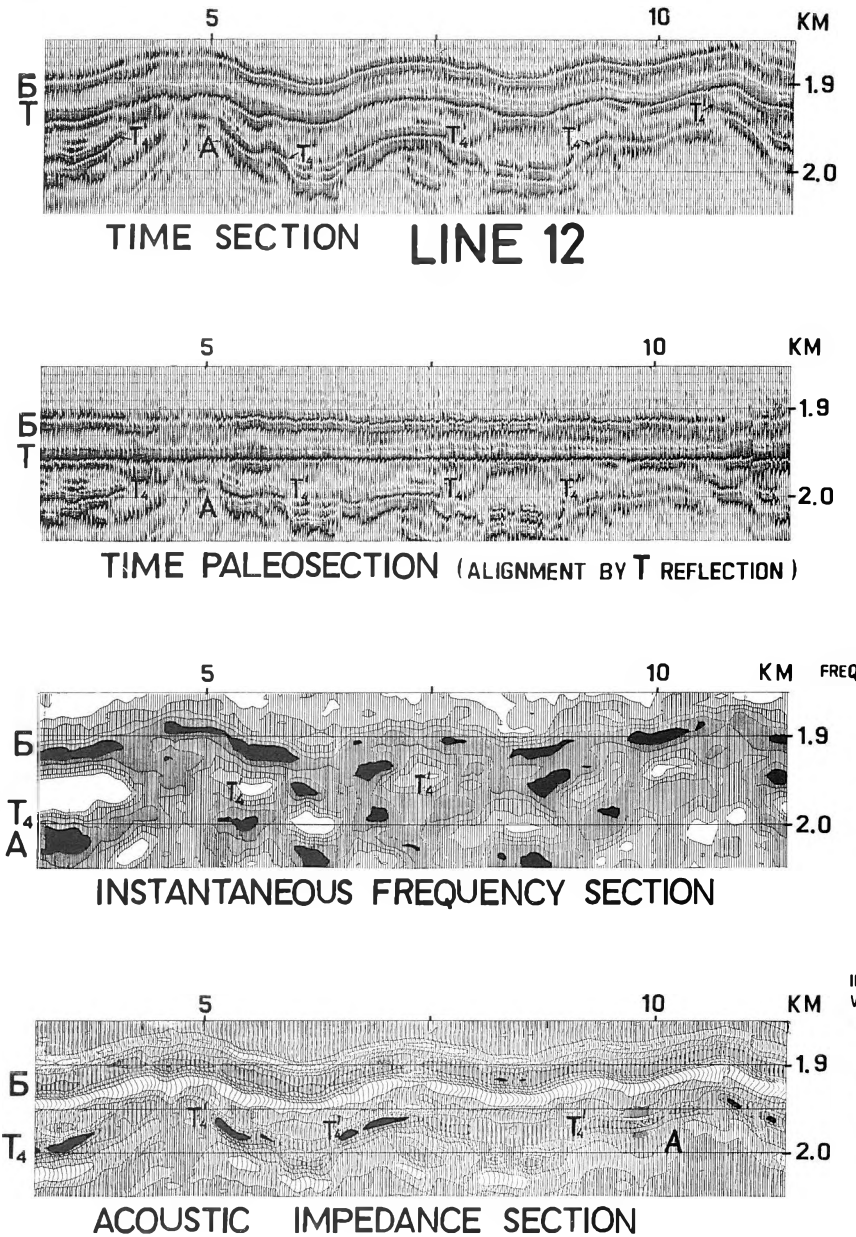

Fig. 14. Example for the extraction of the slope subfacies T'_4

14. ábra. Példa a T'_4 lejtő alfácies kijelölésére

Рис. 14. Пример выделения склоновой субфации T'_4

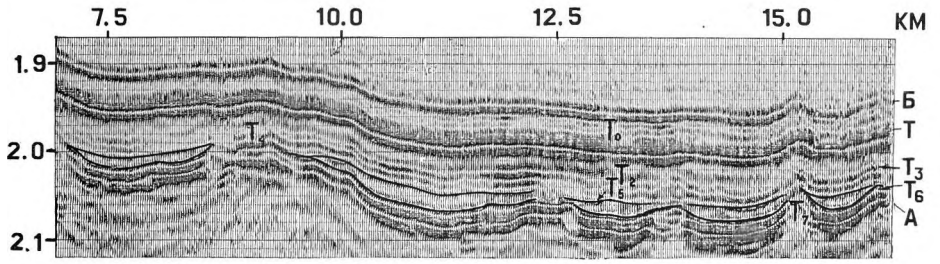

TIME SECTION LINE 5

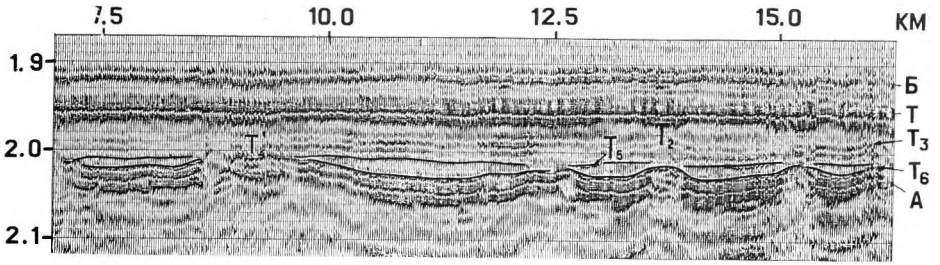

TIME PALEOSECTION (ALIGNMENT BY T REFLECTION)

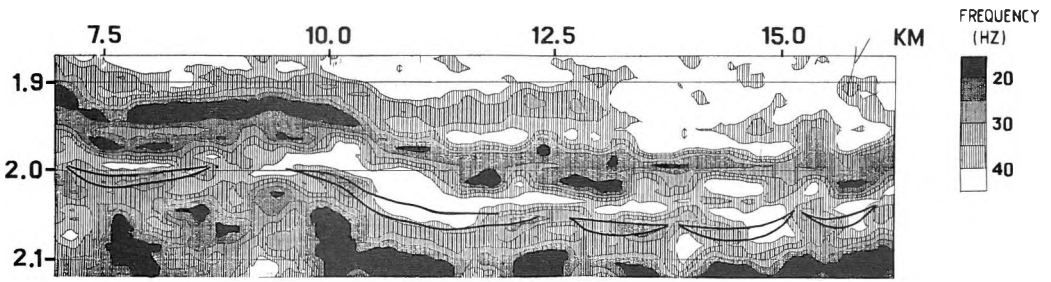

INSTANTANEOUS FREQUENCY SECTION

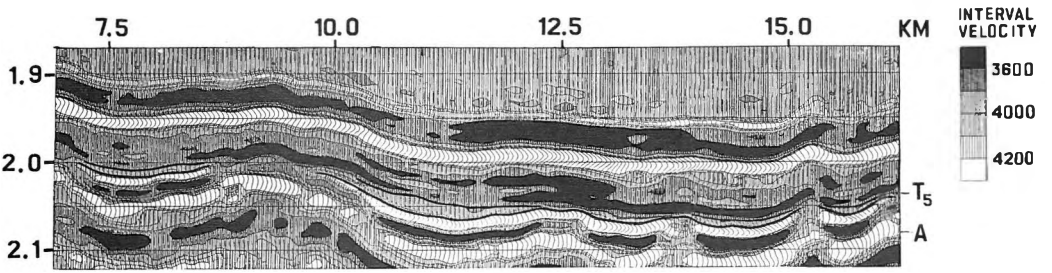

ACOUSTIC IMPEDANCE SECTION

We envisage that increasing the effectiveness of integrated interpretation of seismic- and borehole data may be attained by switching over to 3-dimensional seismics, ensuring to enhance accuracy and detail in mapping of reservoirs. By increasing the number of sonic logging and VSPs the quantitative correlation between seismic- and geological data will improve.

Fig. 15. Appearance of channel fill deposits in the seismic section (subfacies T_6, lenticular seismic facies T_5)

15. ábra. A folyómeder-üledékek reflexióinak megjelenése a szeizmikus anyagban (T_6 alfácies, T_5 lencseszerű szeizmofácies)

Рис. 15. Пример отображения на сейсмических материалах русловых отложений (субфация T_6, линзовидная сейсмофация T_5)

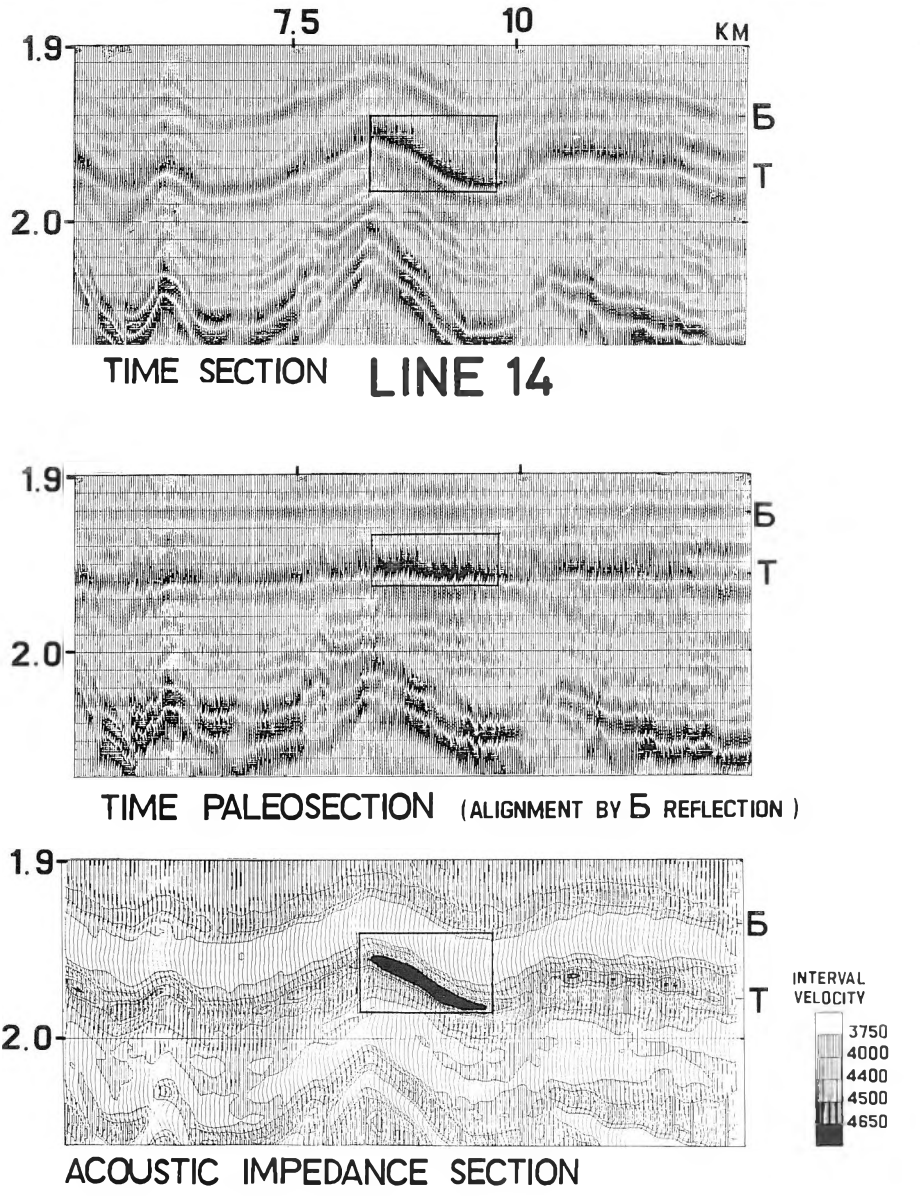

Fig. 16. Extraction of local subfacies connected with increased sand content of the layer at the base of the marine complex (horizon *T*)

16. ábra. Lokális, a réteg elhomokosodásával kapcsolatos alfácies kijelölése a tengeri eredetű összlet feküjében (*T* szint)

Рис. 16. Пример выделения локальной субфации, связанной с опесчаниванием разреза пласта в подножье морского комплекса (горизонт *T*)

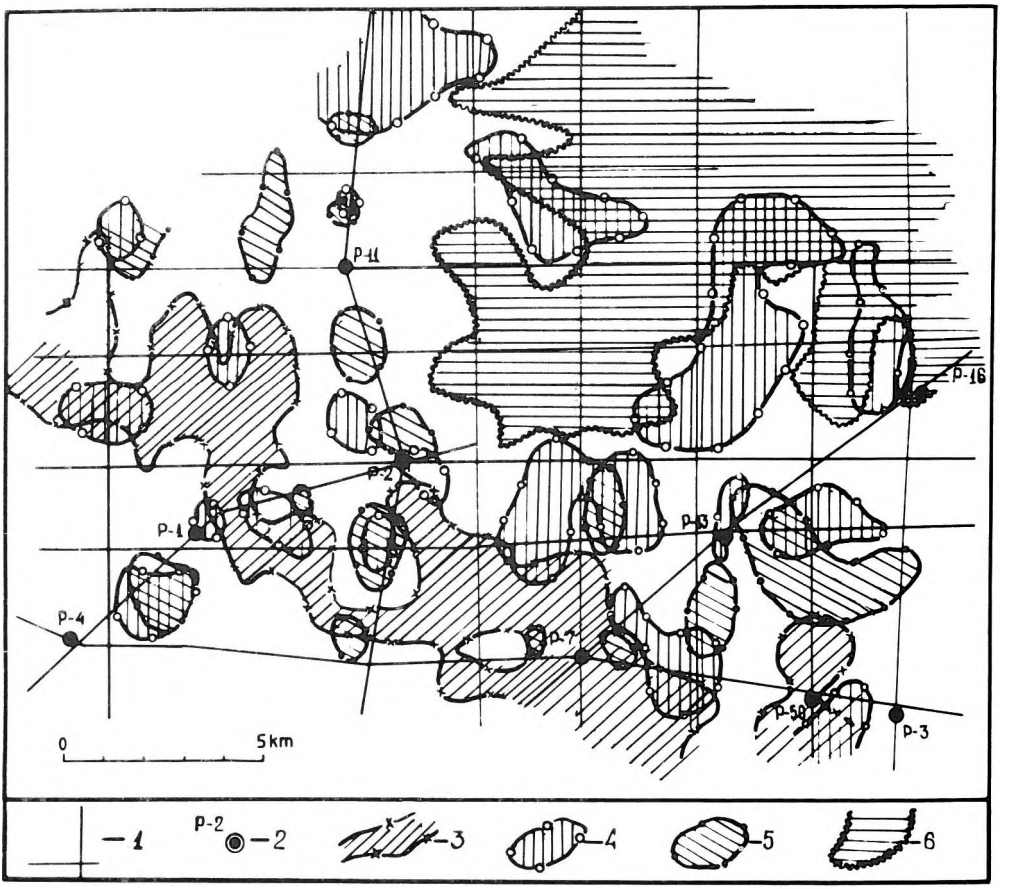

Fig. 17. Distribution of the prospective objects in the investigated area
1—seismic profiles; 2—exploratory boreholes; 3—prospective objects connected with disintegrated basement; 4—prospective objects connected with increased sand content of the layer underlying the marine complex of the Tyumen formation; 5—prospective objects in the proluvial fan deposits; 6—prospective objects connected with alluvial deposits of ancient rivers

17. ábra. A perspektivikus objektumok elhelyezkedésének vázlata a kutatási területen
1—szeizmikus vonalak; 2—kutatófúrások; 3—az aljzat felszínének fellazulásával kapcsolatos perspektivikus objektumok; 4—a tyumeni formáció kontinentális sorozata fedőjének növekvő homoktartalmával kapcsolatos perspektivikus objektumok; 5—a lejtőkön lerakódott hordalékkúpokkal kapcsolatos perspektivikus objektumok; 6—az ősfolyók alluviális üledékeivel kapcsolatos perspektivikus objektumok

Рис. 17. Схема распространения перспективных объектов на площади исследований
1—сейсмические профили; 2—разведочные скважины; 3—перспективные объекты, связываемые с разуплотнением поверхности фундамента; 4—перспективные объекты, связываемые с опесчаниванием разреза в кровле континентальных отложений тюменской свиты; 5—перспективные объекты в делювиально-пролювиальных склоновых отложениях; 6—перспективный объект, связанный с аллювиальными отложениями палеореки

BONYOLULT FELÉPÍTÉSŰ KŐOLAJ- ÉS FÖLDGÁZTÁROLÓK ELŐREJELZÉSE KOMPLEX SZEIZMIKUS–MÉLYFÚRÁSOS VIZSGÁLATTAL

N. A. SZAVOSZT'JANOV, G. N. GOGONENKOV és SZ. SZ. EL'MANOVICS

1. Bevezetés

Az utóbbi időkben az olajipar egyre gyakrabban találja szembe magát azzal a problémával, hogy a szénhidrogének igen bonyolult térbeli alakzatú, inhomogén belső felépítésű tárolókban helyezkednek el. A lelőhelyek szabvány módszerekkel történő feltárása, a készletek számbavétele és a művelés megtervezése kutatófúrások hálózatán alapul, és mint ilyen, igen alacsony hatékonyságú. A tároló felépítésének modellje ugyanis nem felel meg a valóságosnak, ezért a termelőkutak jelentős része nem adja a számított beáramlást. Az ilyen típusú felépítés leggyakrabban a kontinentális összletekben, sekély delta üledékekben és nagy ősföldrajzi lejtőkön fordul elő, ahol az üledékképződés erősen differenciált. A geofizikusok számára jól ismert információ-átviteli terminológiával élve: a kutatófúrások gazdaságilag célszerű sűrűsége nem biztosítja azt a – rétegparaméterek függényeinek leképezéséhez szükséges – mintavételezést, amely kielégítené a Nyquist-feltételt; ennek következtében a keresett függvényeket csak igen nagy hibával állítja elő.

A feladat megfelelő megoldását, szerintünk, a kutatófúrások és a részletező szeizmikus kutatás együttes alkalmazása teszi lehetővé. A terepi mérések technikájában, metodikájában és adatfeldolgozásában az utóbbi 20 évben végbement folyamatos fejlődés lehetőséget biztosít a földtani testek pontos és részletes térképezésére. Bár a szeizmika vertikális irányú felbontóképessége belátható ideig nem éri el a karotázs adatok részletességét, egyre közelebb kerül a rétegek termelési jellemzőinek megadásához. A szeizmika horizontális irányú felbontóképessége azonban már ma is meghaladja a kutatófúrásokét.

Jelen dolgozatban ismertetjük a bonyolult felépítésű tárolók komplex vizsgálatának módszertani alapjait, és egy nyugat-szibériai konkrét kutatási területen, a krasznoleninszki hátságon, bemutatjuk a feladat megoldásának eredményességét is.

A terület szerkezeti viszonyait a szeizmika több mint 10 éve felderítette. Ezután feltáró fúrások ritka hálózatával meghatározták az aljzatközeli, jura időszaki homokos–agyagos összlet regionális olajhozamát. Kiderült, hogy az ezekre az adatokra tervezett további termelőfúrásoknak csak a 30%-a adott a vártnak megfelelő olajbeáramlást. Új termelőfúrások mélyítését leállították, a területet visszaadták további kutatásra. Ennek kapcsán került sor egy szeizmikus vonalhálózat lemérésére, 24-szeres fedéssel *(1. ábra)*.

A regisztrált szeizmikus anyag, a meglevő fúrásokkal és az általános földtani információkkal együtt képezte a komplex kiértékelés alapját. A geológiai–geofizikai információ komplex értelmezésének vázlata a *2. ábrán* látható. Az alkalmazott eljárás legfontosabb sajátossága az értelmezés folyamatában a szeizmikus sztratigráfia elveinek alkalmazása, vagyis keressük azokat az üledékképződési feltételeket, amelyek a reflektáló felületek adott reflexiós hullámképi összességét kialakítják.

A komplex értelmezés egymást követő műveleteit és analízisét könnyen megérthetjük a 2. ábrán feltüntetett vázlat segítségével. Az első lépés a szeizmikus és a fúrási adatok korrelációja. Ehhez szintetikus szeizmogramokat és kétdimenziós modellszámítást alkalmazunk. Miután a szeizmikus szelvény jellemző fázisait azonosítottuk a geológiai határokkal, áttérünk a következő szakaszra – a komplex szeizmosztratigráfiai analízisre – azzal a szándékkal, hogy megszerkesztjük a produktív réteg üledékképződési modelljét. Miután a modellt megszerkesztettük és a tárolók lehetséges változatait számba vettük, hozzáfogunk a potenciális csapdák helyzetének és méreteinek kvantitatív becsléséhez. Végeredményként eljutunk olyan javaslatok kidolgozásához, melyek irányt szabnak a további geofizikai munkákra és a mélyfúrások kitűzésére.

2. A szeizmikus szelvény analízise

Mielőtt áttérnénk az egyes lépések ismertetésére, néhány szót kell szólnunk a szeizmikus adatfeldolgozási és megjelenítési lehetőségekről.

A feldolgozás során nemcsak a zavarok alapos elnyomását kell biztosítani, hanem a szeizmikus regisztrátumok olyan átalakítását, hogy azok mentesek legyenek minden hullámképi jelenségtől: a reflexiós jelek alakja és intenzitása pontosan megfeleljen a földtani szelvény akusztikus sajátságainak. A modern, kellő mélységű feldolgozás – beleértve a valódi amplitúdó-helyreállítást, a szélessávú dekonvolúciót és a migrációt – ezt lehetővé teszi.

A *3. ábra* a kutatási terület egyik tipikus időszelvényét mutatja. A produktív szakaszt nyíl jelöli, felépítése bonyolult, heterogén. A *4. ábrán* szeizmikus időléptékű PS karotázsgörbék vannak az időszelvénybe illesztve. Látható, hogy közvetlenül az aljzat (A) fölött települő összlet a karotázs görbéken gyengén differenciált. A szeizmikus szelvény egyes fázisainak pontos sztratigráfiai azonosítása akusztikus karotázs (AK) alapján történt. Az *5. ábra* az azonosításhoz felhasznált adatrendszert mutatja, összevontan. Középtájt az akusztikus karotázsgörbe foglal helyet, felette sorrendben az impulzus szeizmogram, a szintetikus csatornák, majd egy terepi felvétel csatornái, amelyeket a mélyfúrás közelében regisztráltak. Az AK görbe alatt annak, a szeizmikus felvételezés frekvenciasávjával szűrt változatát, majd a szeizmikus csatornákból, az ismert transzformációval átalakított, pszeudoakusztikus csatornákat ábrázolták.

A szeizmikus kép további, pontosabb azonosítása a földtani szelvénnyel, az egyes reflexiós fázisoknak a konkrét földtani testekkel és ezek együttesével való összekapcsolása a szeizmolitofácies szelvény segítségével történt, melyet a *6. ábrán* láthatunk. A szeizmolitofácies szelvény a szeizmikus időszelvény két, különböző polaritású képének és a mélyfúrási adatoknak együttes ábrázolása. A szeizmikus információ jelenléte lehetővé teszi a mélyfúrások jobb, lényegesen pontosabb korrelálását és ezzel olyan modell létrehozását, amely teljes mértékben összhangban van valamennyi rendelkezésre álló adattal. Ugyancsak lehetőséget nyújt arra is, hogy az egyes tárolók és a szeizmikus reflexiók fázisai közötti kapcsolatot pontosabban határozzuk meg.

Mielőtt a munka következő fázisára áttérnénk, megjegyezzük, hogy ha minden egyes szeizmikus fázis analízisére szükségünk van, akkor az időszelvény szokványos megjelenítési formája nem megfelelő számunkra. Hogy az információt a fekete–fehér szelvényben maximális kompaktsággal ábrázoljuk, kifejlesztettük az általunk kettős polaritású szelvénynek nevezett megjelenítési módot. A *7. ábra* egy részletet mutat az egyik szelvényből, kétféle polaritással, alatta pedig az új ábrázolásmóddal. Látható, hogy a direkt és az inverz polaritás a közeg felépítéséről független információt hordoz, az új eljárás pedig ezt egyesíti, megőrizve mindemellett minden félperiódus valódi polaritásának információját.

3. A földtani modell felállítása

A perspektivikus összlet felépítéséről a szeizmikus fáciesek térbeli modelljének segítségével alkottunk képet *(8. ábra)*. Miután ennek áttekintése nehézkes, egy részét, a nyugat–kelet orientációjú szelvényeket, a *9. ábrán* mutatjuk be. A *10. ábrán* ugyanezen szelvényeket a paleosíkban jelenítjük meg, vagyis a jura utáni tektonikus mozgások hatását vertikális irányú eltolásokkal kiküszöbölve. A szelvényeken az aljzatközeli rész egy alsó, hullámdinamikailag instabil, a fúrási magminták alapján kontinentális üledékre, és egy felső, jelalakja szerint sokkal stabilabb, következésképpen felépítésében is egységesebb részre osztható. Ez utóbbi a fúrási adatok alapján tengeri eredetű üledék. Az összletet genetikailag elválasztó réteghatár a *T* reflexióval azonosítható, amely a transzgresszió során lerakódott alaphomokkőhöz kapcsolódik. Ennek a reflexiónak és a felette elhelyezkedő fázisoknak a jellege arra enged következtetni, hogy a tenger transzgressziójának idejére a kontinentális üledékek gyakorlatilag teljesen kitöltötték a szárazföld mélyedéseit. Éppen emiatt, a paleorekonstrukció a *T* szint alapján készült, a rekonstruált szelvények pedig lehetővé tették az üledékképződési medence ősföldrajzi és paleotektonikai körülményeinek prognosztizálását.

A jura időszak kezdetére a kutatott terület erősen tagolt felszínű szárazulat képét mutatja. A területet délről és nyugatról övező, néhány száz méter magas kiemelkedések erőteljesen erodálódnak, és az üledékanyag a lejtőkön alkalmi homokfolyamok formájában lerakódik. A mélyebb

részeken ártéri, tavi–mocsári üledékek képződnek, vékony széncsíkokkal. Az egész terület lassú süllyedésének folyamán növekszik a kontinentális üledékek vastagsága a közeli kiemelkedések lemosásának és áthalmozásának eredményeképpen. Ezt a folyamatot gyenge tektonikus aktivitás, hajlítások és törések kísérik. A paleovölgyekben, amelyeket szeizmikával könnyen térképezhetünk *(11. ábra)*, kiterjedt folyóhálózatot találunk. Egy meghatározott időpontban az egész medence süllyedése, vagy a tengerszint emelkedése eredményeképpen transzgressziós folyamat indul meg, amelynek következtében lerakódik a tyumeni formáció homokrétege a tengeri sorozat feküjében. A homokkövek vastagsága nagyon változatos. A paleofelszín pozitív alakzataihoz zátonytípusú homoktestek kötődnek. Az e fölött elhelyezkedő réteg homogén, agyagos összetételű, záró fedőréteget alkot. A gyenge tektonikus mozgások folytatódnak, kialakítván az egész üledékes összlet jelenlegi domborzati viszonyait.

A fenti üledékképződési modell segítségével az alábbi főbb potenciális tárolótípusokat különítettük el:

- a törésekkel és mállással fellazított aljzat felszíne a kiemelkedéseken,
- a kiemelkedések lejtőin kifejlődött hordalékkúpok, valamint a lejtő erózióval fellazított felszíne,
- a folyómeder-üledékek (csatornakitöltés) az aljzat legmélyebb részein,
- a zátonyok és csatornák lokális alfáciesei a tyumeni formáció tengeri sorozatában.

4. Perspektivikus testek kijelölése

A kutatott szintek fizikai tulajdonságainak eloszlási sajátosságait a pszeudoakusztikus szelvényekből készített intervallumsebesség-térképek segítségével vizsgáltuk, amelyek alapvető fontosságúak a perspektivikus objektumok kiválasztásában. A szeizmikus- és a termelés-geológiai paraméterek korrelációs kapcsolatának segítségével pedig ezeket az objektumokat térképeztük.

A pszeudoakusztikus sebesség és az aljzat felszínével azonosított *A* szintben levő kutak hozamának elemzése azt a kvalitatív tendenciát jelölte ki, hogy a pszeudosebesség csökkenése a hozamok növekedésével jár. A legperspektivikusabbnak azok a zónák bizonyulhatnak, ahol a sebességérték 3900 m/s vagy ennél kisebb *(12. ábra)*; a csökkent sebességet az aljzatfelszín mállott voltának tulajdonítva. Az *A* szint intervallumsebesség-térképén *(13. ábra)* az ÉNy–DK csapásirányú csökkent sebességű zóna megfelel az aljzat legkiemeltebb helyzetű sávjának és így olajkutatás szempontjából az üledékes takaró aljzatának perspektivikus objektuma.

A lejtőüledékek reflexiós tulajdonságainak vizsgálata során nem sikerült stabil korrelációs kapcsolatot találni a szeizmikus kép dinamikus jellemzői és a kutak hozama között. Ennek ellenére, bár gyakorlatilag valamennyi kút, amelyet a T_4 lejtő alfácies zónájába telepítettek, produktív, a pszeudoakusztikus intervallumsebességek értékei (3150–3500 m/s) csökkenést mutatnak a produktív kutak felé *(14. ábra)*. A perspektivikus objektum kijelöléséhez a T_4 szinten belül a pszeudosebesség küszöbértékét 3400 m/s-nek vettük fel.

A T_6 szubfácies, ill. a T_5 szeizmofácies megnövekedett rétegvastagságú folyómeder üledékeit az intervallumsebességek megnövekedett értékei jellemzik (3950–4050 m/s), amelyek, a modellezés alapján, feltehetően ezen üledékek megnövekedett homoktartalmával vannak összefüggésben *(15. ábra)*.

A tengeri sorozat fekü homokköveivel azonosított *T* horizont részletes vizsgálata, valamint a szeizmikus- és a termelés-geológiai paraméterek korrelációs kapcsolatának meghatározása a területen arra a megállapításra vezetett, hogy a nagy hozamú kutak nagy pszeudoakusztikus intervallumsebesség értékekhez kapcsolódnak. A szeizmikus modellvizsgálatok is azt tükrözték, hogy a produktivitás megnövekedett sebességekkel függ össze. Ezek alapján feltételezhető, hogy az intervallumsebesség (pszeudosebesség) megnövekedett értékeinek helyei *(16. ábra)* megnövekedett homoktartalomnak felelnek meg. Ezáltal javul a réteg tárolóképessége s ennek következtében nő a kút hozama.

Az elvégzett munka eredményeképpen arra a következtetésre jutottunk, hogy a Jem-Jogovszki lelőhely kitermelésére készített eredeti művelési terv nem felel meg a tárolók valódi elrendeződésének, mert nem rétegzett, hajlított szerkezetű lelőhellyel állunk szemben, hanem a produktív objektumok szétszórtak; jelentős részük bonyolult felépítésű, nem antiklinális típusú, különböző eredetű csapda *(17. ábra)*.

A vizsgálatok megmutatták, hogy az általunk kidolgozott, szeizmikus és kútgeofizikai adatok szeizmosztratigráfiai értelmezésére támaszkodó, komplex interpretációs metodika eredményes volt a földtani feladatok megoldásában, a krasznoleninszki hátság bonyolult felépítésű tyumeni formációja esetében. Az eredmények lehetővé tették, hogy javaslatot tegyünk a termelőkutak hálózatának megváltoztatására. Az új fúrási programot két lépcsőben javasoljuk végrehajtani. Az első lépcsőben a kutak közvetlenül a szeizmikus vonalakra települnének. Amennyiben a termelési adatok megerősítik az értelmezés megállapításait, sor kerülhet a termelőkutak rendszerének teljes felülvizsgálatára.

A szeizmikus és a fúrási adatok komplex elemzése hatékonyságának további növelését, hasonló körülmények között, a háromdimenziós szeizmikára való áttérésben látjuk. Ez biztosítaná a bonyolult felépítésű tárolók térképezési pontosságának és részletességének növelését. Az akusztikus karotázs- és a VSP-felvételezések számának növelésével javíthatjuk a szeizmikus adatok és a mélyfúrások által feltárt földtani testek kvantitatív korrelációját.

ПРОГНОЗ СЛОЖНОПОСТРОЕННЫХ КОЛЛЕКТОРОВ КОМПЛЕКСОМ СЕЙСМОРАЗВЕДКИ И БУРЕНИЯ

Н. А. САВОСТЬЯНОВ, Г. Н. ГОГОНЕНКОВ и С. С. ЭЛЬМАНОВИЧ

Рассматриваются вопросы комплексирования данных разведочного бурения и детальной сейсморазведки при изучении сложнопостроенных коллекторов. Изложена методическая основа комплексной интерпретации геолого–геофизических данных с использованием принципов сейсмостратиграфии. Продемонстрирована эффективность решения задачи на примере одной из разведочных площадей Западной Сибири в пределах Красноленинского свода.

GEOPHYSICAL TRANSACTIONS 1986
Vol. 32. No. 1. pp. 31–42

UPWARD CONTINUATION OF UNEVENLY SPACED POTENTIAL FIELD DATA USING EQUIVALENT SOURCES

Marian IVAN*

A complex gravity model is used to compare various upward continuation procedures based on solving integral equations. Such techniques that assume the processed field to be equal to the field of a certain distribution (equivalent source) located on the surface are useless in areas of very rugged topography. Good results are obtained by assuming the observed gravity field to be equal to the potential of a dipole distribution. The relation to the equivalent source concept is a formal one and the equations can be derived from the potential field theory. The accuracy of the results is discussed in relation to the edge effects, the values of the sampling interval, the number of iterations performed and the formula used for approximating the integrals.

Keywords: upward continuation, irregular surfaces, gravity field, integral equations, equivalent sources

1. Introduction

The equivalent source concept has been introduced in order to solve some inverse problems of applied geophysics [e.g. HALL 1958, CORBATÓ 1965, ZIDAROV 1965]. A density (magnetization) distribution is said to be equivalent to a gravity (magnetic) source body when the field of this distribution is equal (or very close in actual cases) to the observed field on the topographic surface. The goodness of fit is the only actual criterion on the reliability of this equivalent source if other geological or geophysical data are not used as constraints. The main problem of data processing by such procedures is to select the proper location for the equivalent sources. If the mass points (magnetic dipoles) are placed too far below (or too close to) the topographic surface, the equivalent source is unstable and so it cannot be used for data processing [DAMPNEY 1969, EMILIA 1973].

Despite the above, BHATTACHARYYA and CHAN [1977] proposed a technique for the upward continuation between irregular surfaces of potential field data (Dirichlet problem) based on equivalent sources located just on the surface. In the 2-D case, the gravity field of the source body is assumed to be equal to the field of a surface mass distribution at all the points situated above and on the surface, i.e.

* University of Bucharest, Geoph. Labs., Str. Traian VUIA 6, 70139 Bucharest 39, Romania
Manuscript received: 26 August, 1985

$$g(\bar{x}, H) = \int_{(T)} \frac{\sigma(x, h(x))\,(H - h(x))\,\mathrm{d}x}{(\bar{x} - x)^2 + (H - h(x))^2}, \tag{1}$$

where

$$\sigma = 2G\varrho\sqrt{1 + (\mathrm{d}h/\mathrm{d}x)^2}, \tag{2}$$

ϱ = linear density distribution on the surface
and G = gravitational constant.
The topographic profile (T) is positive upward, defined as

$$z = h(x). \tag{3}$$

The distribution is obtained by solving iteratively the Fredholm integral equation

$$\sigma(\bar{x}, h(\bar{x})) = \frac{1 + (\mathrm{d}h/\mathrm{d}\bar{x})^2}{\pi}\left[g(\bar{x}, h(\bar{x})) - \int_{(T^*)} \frac{\sigma(x, h(x))\,(h(\bar{x}) - h(x))\,\mathrm{d}x}{(\bar{x} - x)^2 + (h(\bar{x}) - h(x))^2} \right], \tag{4}$$

where (T^*) represents the surface without the point of coordinates $(\bar{x}, h(\bar{x}))$. The upward continued field is then obtained by using Eq. (1).

For magnetic data processing, a dipole (normal to the relief) distribution is similarly assumed such that its field F is equal to the observed field everywhere above and on the surface. The corresponding integral equation is

$$\mu(\bar{x}, h(\bar{x})) = \frac{1}{\pi}\left[F(\bar{x}, h(\bar{x})) - \int_{(T^*)} \mu(x, h(x)) \frac{-(\bar{x} - x)\,\mathrm{d}h/\mathrm{d}x + h(\bar{x}) - h(x)}{(\bar{x} - x)^2 + (h(\bar{x}) - h(x))^2}\,\mathrm{d}x \right]. \tag{5}$$

Then

$$F(\bar{x}, H) = \int_{(T)} \mu(x, h(x)) \frac{-(\bar{x} - x)\,\mathrm{d}h/\mathrm{d}x + H - h(x)}{(\bar{x} - x)^2 + (H - h(x))^2}\,\mathrm{d}x. \tag{6}$$

A significant difference appears between the above relationships. In Eq. (1), the gravity field of the source body is assumed to be equal to the field of a mass distribution (i.e. a true equivalent source). In Eq. (6), the anomalous field is equal not to the field but to the potential of a magnetic dipole distribution. The convergence properties of Eqs. (4) and (5) are consequently expected not to be the same. KELLOG [1953] simply solves the Dirichlet problem without using the above equivalent source concept. By representing any potential field by Eq. (6), the unknown function μ results immediately from Eq. (5) which is just the limiting value of the dipole source potential when the observation point approaches the surface along the normal. At least in this case, the relation between the equivalent source concept and the upward continuation problem seems to be a formal one.

Actually, a finite number of observation points is available so that the equivalent distribution is a discrete one. Consequently, Eq. (1) and its magnetic equivalent are solvable as Fredholm integral equations of the first kind.

According to the uniqueness of the Dirichlet problem solution, no matter what kind of integral equation is solved and irrespective of the gravity or magnetic nature of the processed potential field, the same upward continued values are expected to be obtained. By assuming that the right side of Eq. (1) is the magnetic potential of a vertical dipole distribution, NAKATSUKA [1981] consequently processed a magnetic field by using Eq. (4). HANSEN and MIYAZAKI [1984] processed a magnetic field with Eq. (5) and outlined too that this relation can be used for the upward continuation of other potential fields.

When actual fields are processed, the finite number of measurements and the topographical irregularities have a substantially different impact upon the above techniques so that unreal results may often be obtained.

In this paper, a complex gravity model is used to compare various upward continuation procedures based on solving integral equations. The accuracy of the results is discussed in relation to the edge effects, the values of the sampling interval, the number of iterations performed and the formula used for approximating the integrals.

2. The model

The assumed topographic relief is given by

$$h(x) = 600/(p + (x/75)^2). \tag{7}$$

The parameter is set to $p = 3$. The source body is represented by three horizontal infinite cylinders *(Fig. 1)*. Its gravity field is represented by

$$g(x, z) = \sum_{i=1}^{3} m_i(z - z_i)/(x^2 + (z - z_i)^2), \tag{8}$$

where

$$m_1 = 50 \qquad m_2 = 112.5 \qquad m_3 = 200$$

and

$$z_1 = 125 \qquad z_2 = 0 \qquad z = -175.$$

This field has been sampled at the points having the x-coordinates equal to

$$x_k = \pm 25(k - 1) \qquad k = 1, \ldots, 25. \tag{9}$$

The lengths are given in meters and the field is in mGals.

In order to minimize the truncation effect, a horizontal infinite cylinder has been found such that its field is very close at the edges of the topographic profile to the field of Eq. (8) [IVAN in press]. Its field is

$$g_c(x, z) = 212.75(z + 135.48)/(x^2 + (z + 135.48)^2). \tag{10}$$

This field is then subtracted from that of the source body and the result is continued upward to the desired level. The values of g_c at the same level are finally summed.

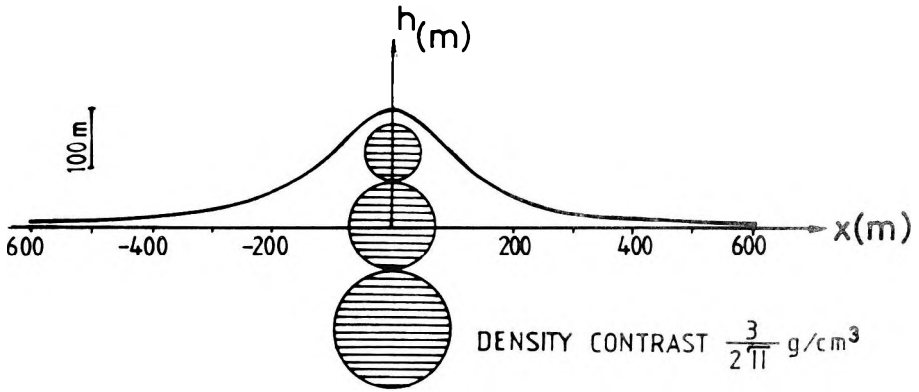

Fig. 1. Topographic profile with the source body

1. ábra. Topográfiai szelvény a hatóval

Рис. 1. Профиль с изображением рельефа и возмущающего тела

3. Data processing using Fredholm integral equations of the first kind

Infinite horizontal mass lines have been placed on the topographic profile at each point of the initial x-coordinates equal to

$$x_j = \pm(25j - 12.5) \qquad j = 1, \ldots, 24. \tag{11}$$

The field at point (x, z) due to the mass line placed at $(x_j, h(x_j))$ is

$$g_j(x, z) = S_j \Delta z / (\Delta x^2 + \Delta z^2), \tag{12}$$

where

$$\Delta x = x - x_j$$

and

$$\Delta z = z - z_j.$$

An iterative procedure was used in an endeavour to find the values of S_j and x_j so that the total field due to the mass lines distribution be as close as possible in the sense of least squares to the sampled field of Eq. (8). Different sets of values are obtained without a definite trend towards a certain distribution *(Table I/a)*. All of them give a good fit to the sampled field on the topographic profile *(Fig. 2)*. Their field above the relief has the same values for all these distributions but it is quite different from the exact values *(Fig. 3)*. Both the fit

(a)	$\pm x_j$	13	35	62	87	112	137	162	187	212	237	262	287	312	336	361	386	411	435	460	484	509	532	555	579
	S_j	0.4	3.1	6.1	7.1	7.5	8.3	9.3	10.7	12.5	14.7	17.4	20.6	24.4	28.7	33.7	39.2	45.6	52.5	60.7	68.2	81.1	81.9	71.2	78.6
(b)	$\pm x_j$	12.5	37.5	62.5	87.5	112.5	137.5	162.5	187.5	212.5	237.5	262.5	287.5	312.5	337.5	362.6	387.5	412.6	437.5	462.6	487.5	512.6	537.5	562.7	587.5
	D_j	103	245	312	227	166	102	73	49	39	30	24	21	16	16	11	13	8	12	5	11	3	10	1	10

Table I. Parameters of a simple- (a) and of a dipole- (b) source distribution. The edge effect is neglected

I. táblázat. Egyszerű- (a) és dipól- (b) hatóeloszlás paraméterei. A peremi hatás elhanyagolva

Таблица I. Распределение параметров над простым (a) и дипольным (b) возмущающим телом. Краевые влияния пренебрегаются

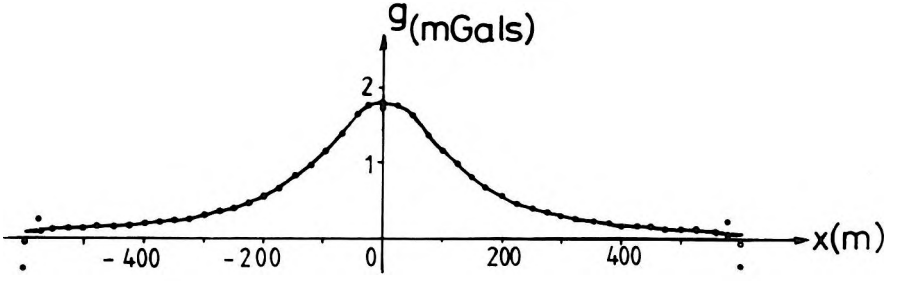

Fig. 2. Gravity fields along the topographic profile of Fig. 1. The solid line shows the field of the body; the filled circles are the values of the field due to the simple equivalent source from Table I/a; the empty circles are the same values when the edge effect is reduced

2. ábra. A gravitációs tér értékei az 1. ábra topográfiai szelvénye mentén. A folytonos vonal a ható tere, a pontok az I/a táblázatból vett egyszerű ekvivalens ható által létrehozott tér értékeit mutatják; a körök ugyanezen értékek, a peremi hatás csökkentésével

Рис. 2. Значение поля силы тяжести вдоль профиля, изображенного на рис. 1. Непрерывной линией показано поле от возмущающего тела, точками изображается поле силы тяжести от простого эквивалентного возмущающего тела, значения которого взяты из таблицы I/a; кружками обозначены те же значения, уменьшенные на краевой эффект

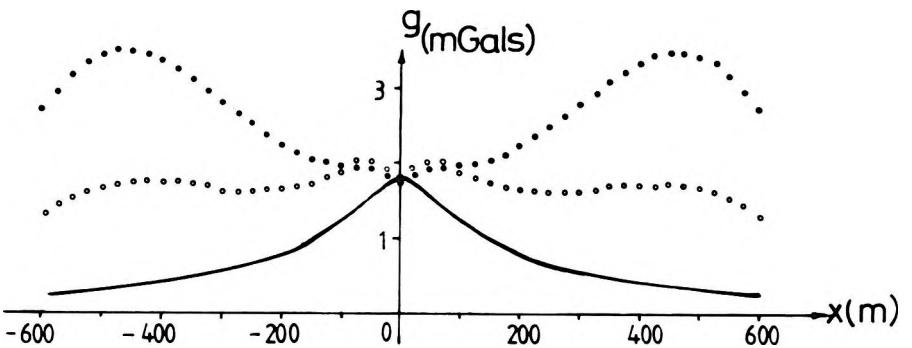

Fig. 3. Gravity fields on the plane at a height of 200 m. For legend, see Fig. 2

3. ábra. Térerősség értékek a 200 m magasságban levő síkon. Jelölések: mint a 2. ábrán

Рис. 3. Значения потенциального поля в плоскости на высоте 200 метров. Обозначения такие же, как на рис. 2.

and the upward continued values are improved when the edge effect is minimized but the differences with respect to the field of the body are significant even at great elevations *(Fig. 4)*.

In a second approach, the above mass lines have been replaced by dipoles having their axes normal to the relief. The field at point (x, z) due to the dipole placed at $(x_j, h(x_j))$ is

$$F_j(x, z) = D_j(\Delta x^2 - \Delta z^2 + 2\Delta x \Delta z \, \mathrm{d}h/\mathrm{d}x_j)/(\Delta x^2 + \Delta z^2)^2/\sqrt{1 + (\mathrm{d}h/\mathrm{d}x_j)^2}. \quad (13)$$

The above procedure now seems to be stable and the field of the obtained distribution *(Table I/b)* gives a remarkably good fit to the sampled field of Eq. (8) so that the maximum deviation is less than 0.01 mGal. But the field of this equivalent source almost vanishes above the relief so that a negative anomaly having its amplitude equal to -0.02 mGals is obtained on the plane at a height of 350 m. The minimization of the edge effect gives only a formal improvement.

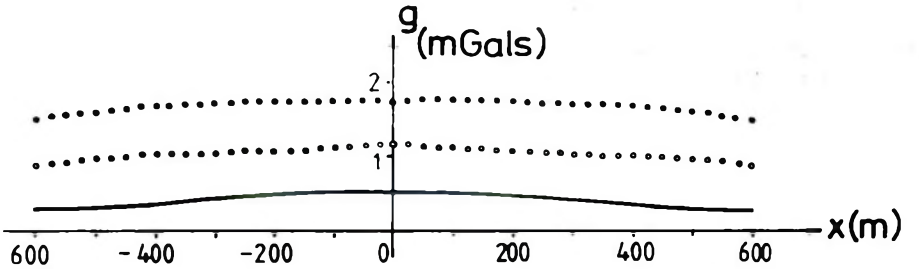

Fig. 4. Gravity fields on the plane at a height of 650 m. For legend, see Fig. 2

4. ábra. Térerősségértékek a 650 m magasságban levő síkon. Jelölések: mint a 2. ábrán

Рис. 4. Поле силы тяжести на высоте 650 метров. Обозначения такие же, как на рис. 2.

4. Data processing using Fredholm integral equations of the second kind

The sampled field of Eq. (8) has been processed by using Eqs. (4) and (1) in order to obtain the upward continued values at certain levels. The derivatives have been computed by differentiating Eq. (7). The integrals were evaluated by using a simple sum (the linear trapezoidal formula). *Figure 5* shows the failure of Eq. (4) to obtain convergence. No improvement appears even when the edge effect is minimized and the observed field is sampled at an interval of 5 m.

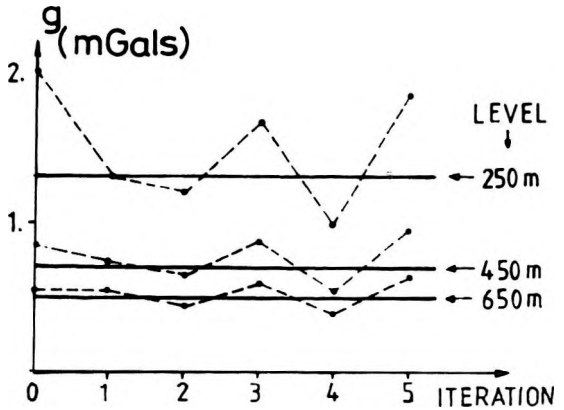

Fig. 5. Central values of upward continued field obtained by using Eqs. (4) and (1) at different levels and iterations (dashed lines). Exact values are represented by solid lines

5. ábra. A (4) és (1) egyenlettel számított fölfelé folytatott tér középponti értékei, különböző szintekre, és iterációkkal (szaggatott vonal). A pontos értékeket a folytonos vonalak jelölik

Рис. 5. Средние центральные значения поля, продолженного вверх на различные уровни, рассчитанные по уравнениям (1) и (4) с итерациями (прерывистая линия). Точные значения указаны сплошной линией

Convergent results are always obtained by using Eqs. (5) and (6) so that only 3 or 4 iterations are needed. By setting $p=2$ in Eq. (7) a more rugged relief results *(Fig. 6)*. The observed field is now clearly disturbed *(Fig. 7)* and an upward continuation becomes really necessary. The gravity values sampled at various intervals have been continued to planes located at different heights above the relief. The results are unreal when these planes are placed near the top of the relief so that the minimum height seems to be around twice the sampling interval.

A more careful evaluation of the integrals has been used [HANSEN and MIYAZAKI 1984] with good results. In this case, the computer time necessary is essentially increased with respect to the simple summing formula. The value of the sampling interval has an important impact on the accuracy of the upward continued field and the errors are reduced to almost half their value when the edge effect is minimized *(Fig. 8)*.

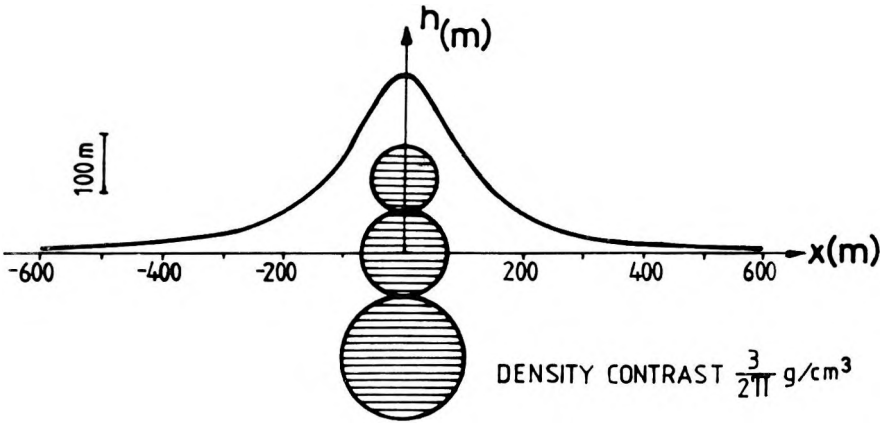

Fig. 6. A more rugged topographic relief with the source body

6. ábra. Erősebben tagolt topográfiai szelvény a hatóval

Рис. 6. Профиль с сильно изрезанным рельефом, показано положение возмущающего тела

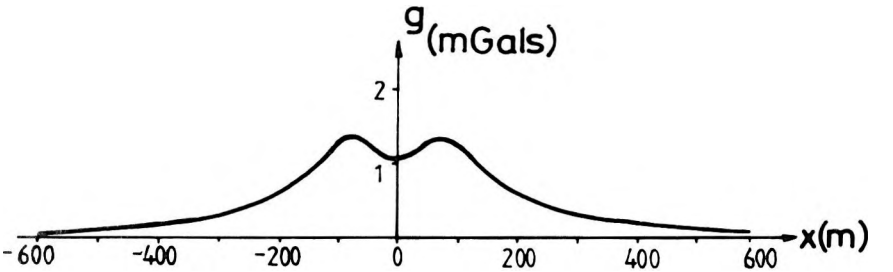

Fig. 7. Gravity field along the topographic profile of Fig. 6

7. ábra. Gravitációs tér a 6. ábrán bemutatott topográfiai szelvény mentén

Рис. 7. Поле силы тяжести вдоль профиля, приведенного на рис. 6.

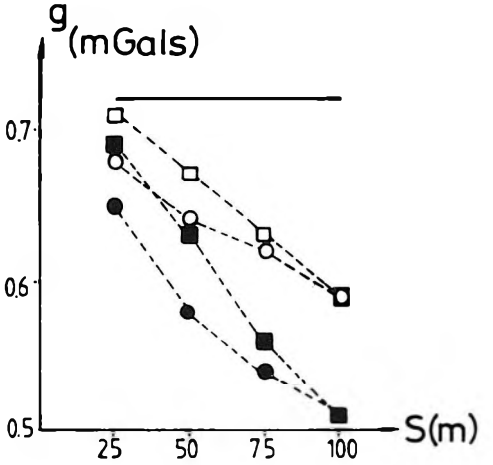

Fig. 8. Central values of upward continued field on the plane at a height of 450 m versus the value of the sampling interval. The integrals are evaluated by using the HANSEN and MIYAZAKI [1984] formula (squares) and by simple summing (circles). The filled circles and squares show the values obtained when the edge effect is not reduced, the empty circles and squares show the same values obtained when the edge effect is minimized. The solid line represents the exact value

8. ábra. A felfelé folytatott tér középponti értékei a 450 m magasságban levő síkon, a mintavételi köz függvényében. A függvényértékeket kiszámítottuk HANSEN és MIYAZAKI [1984] képletével (négyzetek) és egyszerű összegezéssel (körök). A tele körök és négyzetek jelölik a peremhatás figyelembevétele nélküli értékeket, az üres körök és négyzetek pedig ugyanezen értékeket, a peremhatás minimalizálásával. A folytonos vonal a pontos értéket adja

Рис. 8. Средние центральные значения поля, продолженного вверх на высоту 450 метров, в зависимости от расстояния между точками наблюдения. Значения рассчитаны по уровнениям ХАНСЕНА и МИЯЗАКИ [1984] (по квадратам) и простым суммированием (по кругам). Зачерненные круги и квадраты обозначают значения, полученные без учета краевых влияний, а пустые круги и квадраты при их учете. Сплошной линией показаны точные значения

5. Conclusions

All procedures assuming the processed field to be equal to the field of a certain source distribution placed on a rugged topography are useless for the upward continuation. Good results are obtained by using the potential of a dipole distribution but the relation to the equivalent source concept is a formal one and the equations are immediately derived from potential field theory. Due both to the value of the sampling interval and the edge effects, only qualitative results are expected to be obtained in many actual cases.

One of the main problems of upward continuation procedures is the great amount of computations required especially when surface data are processed.

In view of this, the simplest evaluation of the integrals is desirable. Numerical tests have indicated that the zero-order approximation of Eq. (5) always restores the correct shape of the gravity field by erasing the disturbing effects of the topography. This formula also represents an approximate generalization of the plane Dirichlet integral [GRANT and WEST 1965] valid for the upward continuation between irregular surfaces of any potential field data [IVAN in press]. Bearing in mind that upward continuation is only an intermediate stage towards source modelling, it sometimes seems desirable to limit ourselves to performing this procedure only.

REFERENCES

BHATTACHARYYA B. K., CHAN K. C. 1977: Reduction of magnetic and gravity data on an arbitrary surface acquired in a region of high topographic relief. Geophysics **42,** 7, pp. 1411–1430

CORBATÓ C. E. 1965: A least-squares procedure for gravity interpretation. Geophysics **30,** 2, pp. 228–233

DAMPNEY C. N. G. 1969: The equivalent source technique. Geophysics **34,** 1, pp. 39–53

EMILIA D. A. 1973: Equivalent sources used as an analytic base for processing total magnetic field profiles. Geophysics **38,** 2, pp. 339–348

GRANT F. S., WEST G. F. 1965: Interpretation theory in applied geophysics. McGraw Hill, New York

HALL D. H. 1958: Least squares in magnetic and gravity interpretation. Trans. Am. Geophys. Union **39,** 1, pp. 35–39

HANSEN R. O., MIYAZAKI Y. 1984: Continuation of potential fields between arbitrary surfaces. Geophysics **49,** 6, pp. 787–795

IVAN M. (in press): On the upward continuation of potential field data between irregular surfaces. Geophys. Prosp.

KELLOG O. D. 1953: Foundations of potential field theory. Dover Publ., New York

NAKATSUKA T. 1981: Reduction of magnetic anomalies to and from an arbitrary surface. Butsuri-Tanko **34,** pp. 6–12

ZIDAROV D. 1965: Solution of some inverse problems of applied geophysics. Geophys. Prosp. **13,** 2, pp. 240–246

SZABÁLYTALAN MINTAVÉTELEZÉSŰ POTENCIÁLTÉR FELFELÉ FOLYTATÁSA EKVIVALENS HATÓK ALKALMAZÁSÁVAL

Marian IVAN

Több hatóból álló gravitációs modellt alkalmaztunk az integrál egyenleteket felhasználó különféle fölfelé folytató eljárások összehasonlítására. Ezek az eljárások feltételezik, hogy a fölfelé folytatott tér megegyezik egy alkalmasan választott felszíni eloszlás (az ún. ekvivalens ható) terével. Erősen tagolt topográfiájú területeken ez az eljárás nem válik be. Jó eredményeket kaphatunk annak feltételezésével, hogy az észlelt gravitációs tér megegyezik egy dipól eloszlás potenciáljával. Az egyenletek levezethetők a potenciáltér elméletéből, ezért az ekvivalens ható fogalmának használata pusztán formális. A cikk részletezi, hogy az eredmények pontossága miként függ a peremhatásoktól, a mintavételi távolságtól, az elvégzett iterációk számától és az integrálok megközelítésének módjától.

АНАЛИТИЧЕСКОЕ ПРОДОЛЖЕНИЕ НЕРАВНОМЕРНО ИЗМЕРЕННОГО ПОЛЯ СИЛЫ ТЯЖЕСТИ В ВЕРХНЕЕ ПОЛУПРОСТРАНСТВО С ПРИМЕНЕНИЕМ ЭКВИВАЛЕНТНЫХ ВОЗМУЩАЮЩИХ ТЕЛ

Мариан ИВАН

В целях сравнения различных способов продолжения поля потенциалов силы тяжести в верхнее полупространство использовалась модель, состоящая из нескольких возмущающих тел. Обычно, при рассчетах этими способами, предполагается, что поле, продолженное в верхнее полупространство, совпадает с наблюдаемым на поверхности от выбранного (так наз. эквивалентного) возмущающего тела. В случае сильно изрезанного рельефа этот метод дает большие ошибки. Хорошие результаты получаются, если предположить, что наблюдаемая аномалия гравитационного поля совпадает с распределением потенциального поля от диполя. Уравнения выводятся из теории поля, поэтому применение термина эквивалентного возмущающего тела пустая формальность. В статье подробно рассматривается каким образом на точность результатов влияют краевые условия, расстояния между пунктами наблюдений, зависимость результатов от числа итераций и от метода приближения интегралов.

GEOPHYSICAL TRANSACTIONS 1986
Vol. 32. No. 1. pp. 43–56

FIELD OF A VERTICAL, ALTERNATING CURRENT, ELECTRIC ELEMENTARY DIPOLE IN A LAYERED MEDIUM

Ernő TAKÁCS*, Jenő NAGY*, and Ferenc MÁDAI*

Formulae are derived for the field-strength components of a vertical, alternating current, elementary electric dipole in a layered medium where the measurement point is placed inside an arbitrary layer. The formulae are applied to compute field-strength and apparent resistivity curves with respect to the vertical electric component which can be measured in the equatorial plane of the dipole, between an infinitely extended underlying and overlying layer.

Keywords: electric elementary dipole, frequency sounding, layered medium, geolectric transmission method, in-seam geoelectric measurements, coal mines

1. Introduction

Recently, because of the increasing popularity of geoelectric methods in mines, we frequently face problems which call for the computation of the field of a dipole placed between bedrock and overburden. The Department of Geophysics of the Technical University for Heavy Industry has many times been contracted to apply transmission methods between boreholes and mining spaces in order to determine the local distribution of the physical properties within the rock mass and their temporal changes; to investigate the bedrock and the roof of coal seams; to locate the boreholes from the mining space. All these tasks require a knowledge of the electromagnetic field of the dipole in a full space [TAKÁCS 1979].

2. Mathematical considerations

Let us place a vertical elementary electric dipole in a horizontally layered infinite space. Let the origin of the Cartesian system of coordinates agree with the position of the dipole such that the dipole moment should point vertically downwards in the direction of the z axis. Each layer is homogeneous and isotropic in itself, its magnetic permeability is μ_0, its wave number due to dielectric permittivity can be neglected at the applied frequency. Its conductivities are $\sigma_1, \sigma_2, \ldots \sigma_p \ldots \sigma_N$ and $\sigma_1^*, \sigma_2^*, \ldots \sigma_p^* \ldots \sigma_N^*$, respectively, independently of frequency *(Fig. 1)*.

* Department of Geophysics, Technical University for Heavy Industry, Miskolc, Egyetemváros, H–3515, Hungary Manuscript received (revised form) 30 July, 1985

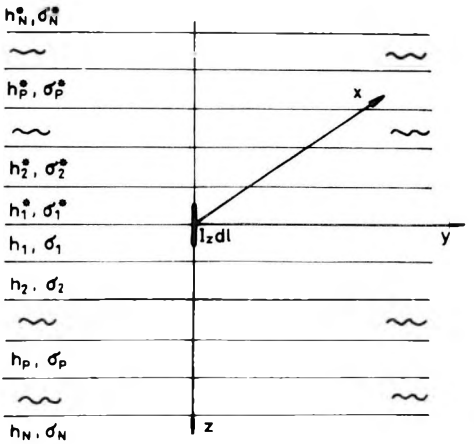

Fig. 1. Vertical electric elementary dipole in a layered medium

1. ábra. Vertikális elektromos elemi dipólus rétegzett közegben

Рис. 1. Вертикальный элементарный электрический диполь в слоистой среде

Taking into account the circular rotational symmetry around the z axis, for any given layer the electromagnetic field components can be computed from the expression for the z-oriented vector potential A_{zp} [KAUFMAN 1970]:

$$A_{zp} = \frac{I_z\, dl\mu_0}{4\pi} \int_0^\infty W_p(z)\, J_0(mr)\, \mathrm{d}m, \tag{1}$$

where $p = 1, 2, \ldots, N$ is the serial number of the layer,

$I_z\, dl$ is the current moment of the dipole,

r is the horizontal distance from the z axis, $r^2 = x^2 + y^2$,

$W_p(z)$ and $J_0(mr)$ are the general solutions to the two one-variable differential equations deduced by means of separating the variables in the differential equation for the vector potential A_{zp} derived from Maxwell's equation,

m is an auxiliary variable,

$J_0(mr)$ is a Bessel function of the first kind.

In what follows we shall use the notation $M = \dfrac{I_z\, dl\mu_0}{4\pi}$.

Because of the circular symmetry the magnetic field-strength, H possesses a single (in terms of a cylindrical system of coordinates, φ-directed) component, i.e. it is related to A_{zp} as

$$H_p = -\frac{1}{\mu_0} \frac{\partial A_{zp}}{\partial r}. \tag{2}$$

The electric field strength has only radial and z-directed components, given by

$$E_{rp} = -\frac{\mathrm{i}}{k_p^2}\frac{\partial^2 A_{zp}}{\partial z \partial r} \tag{3}$$

$$E_{zp} = \mathrm{i}\omega A_{zp} - \frac{\mathrm{i}\omega}{k_p^2}\frac{\partial^2 A_{zp}}{\partial z^2} \tag{4}$$

where

$$k_p^2 = \mathrm{i}\omega\mu_0\sigma_p \tag{5}$$

is the wave number inside the layer.
The function W_p figuring in the expression for A_{zp} satisfies the differential equation

$$\frac{\partial^2 W_p}{\partial z^2} - a_p^2 W_p = 0$$

which has the solution

$$W_p = g_p \mathrm{e}^{a_p z} + b_p \mathrm{e}^{-a_p z}.$$

$$a_p = \sqrt{m^2 + k_p^2} \quad \text{and} \quad \operatorname{Re} a_p > 0. \tag{6}$$

In what follows we shall mainly be concerned with the determination of the coefficients g_p and b_p. Let us first assume that the transmitter is placed at $z = +0$. Taking into account the behaviour of the electromagnetic field components at such layer boundaries which do not contain sources, and considering the outer layers as infinite half-spaces, the following equations can be written for coefficients g_1 and b_1:
Defining the quantities R_p as

$$R_p = -\frac{a_p W_p}{\partial W_p/\partial z}$$

we have for $z = +0$

$$\frac{b_1 + g_1}{b_1 - g_1} = R_1. \tag{7}$$

Similarly, for factors g_1^* and b_1^* we have for $z = -0$

$$\frac{b_1^* + g_1^*}{b_1^* - g_1^*} = -R_1^*. \tag{8}$$

with $R_p^* = \dfrac{a_p^* W_p^*}{\partial W_p^*/\partial z}$.

Since for $z>0$ we have N layers, of respective thickness h_1, h_2, ..., h_n and conductivities σ_1, σ_2, ... σ_N; the value of R_1 can be computed from:

$$R_1 = \operatorname{cotanh}\left\{a_1 h_1 + \operatorname{ar\,cotanh}\left[\frac{a_1\sigma_2}{a_2\sigma_1}\operatorname{cotanh}\left(a_2 h_2 + \ldots\right.\right.\right.$$

$$\left.\left.\left. \ldots + \operatorname{ar\,cotanh}\frac{a_{N-1}-\sigma_N}{a_N\sigma_{N-1}}\right)\right]\right\} \tag{9}$$

In the case $z<0$ there are N^* layers and similar equations hold for R_1^*, with the values a_p^*, h_p^* and σ_p^* instead of the previously used ones. Here, we make use of the fact that in the bedrock $R_N=1$, whereas in the roof $R_N^*=-1$.

For the determination of b_1, g_1, b_1^*, g_1^* the source-condition should also be taken into account at the boundary $z=+0$, containing the source. Since the conductivities of the layers on the two sides of this boundary are σ_1 and σ_1^*, respectively, we have

$$\frac{a_1}{k_1^2}(g_1-b_1) - \frac{a_1^*}{k_1^{*2}}(g_1^*-b_1^*) = -\frac{2m}{k_1^2} \tag{10}$$

At $z=0$ the continuity of W and W^* implies

$$b_1+g_1 = b_1^*+g_1^*. \tag{11}$$

On the basis of Eqs. (7), (8), (10), (11), for the computation of W_1 directly below the plane $z=0$, and of W_1^* directly above this plane, one should utilize the coefficients

$$b_1 = \frac{m/k_1^2}{\dfrac{a_1^*}{k_1^{*2}}\dfrac{1}{R^*}+\dfrac{a_1}{k_1^2}\dfrac{1}{R}}\left(1+\frac{1}{R_1}\right) = C\left(1+\frac{1}{R_1}\right), \tag{12}$$

$$g_1 = C\left(1-\frac{1}{R_1}\right), \tag{13}$$

$$b_1^* = C\left(1-\frac{1}{R_1^*}\right), \tag{14}$$

$$g_1^* = C\left(1+\frac{1}{R_1^*}\right). \tag{15}$$

From a knowledge of these coefficients, the vector potentials A_{z1}, A_{z1}^* in the layers immediately below and above the plane $z=0$, respectively, can be expressed and the field components computed from Eqs. (2) and (3).

In order to compute the electromagnetic field components in the other layers, we write down the conditional equations for the layer boundaries and solve them for the coefficients. For the p-th layer:

$$g_p = \frac{1}{2} e^{-a_p(h_1+\ldots+h_{p-1})}\left[g_{p-1} e^{a_{p-1}(h_1+\ldots+h_{p-1})}\left(1+\frac{a_{p-1}}{a_p}\frac{k_p^2}{k_{p-1}^2}\right)+\right.$$
$$\left.+ b_{p-1} e^{-a_{p-1}(h_1+\ldots+h_{p-1})}\left(1-\frac{a_{p-1}}{a_p}\frac{k_p^2}{k_{p-1}^2}\right)\right] \tag{16}$$

$$b_p = \frac{1}{2} e^{a_p(h_1+\ldots+h_{p-1})}\left[g_{p-1} e^{a_{p-1}(h_1+\ldots+h_{p-1})}\left(1-\frac{a_{p-1}}{a_p}\frac{k_p^2}{k_{p-1}^2}\right)+\right.$$
$$\left.+ b_{p-1} e^{-a_{p-1}(h_1+\ldots+h_{p-1})}\left(1+\frac{a_{p-1}}{a_p}\frac{k_p^2}{k_{p-1}^2}\right)\right] \tag{17}$$

For the layers above the $z=0$ plane the coefficients are obtained by substituting the values marked by "*" into Eqs. (16) and (17). For the computation of the field characteristics, according to Eqs. (2) and (3) we also need the derivatives of A_{zp} with respect to r and z:

$$\frac{\partial A_{zp}}{\partial r} = M\int_0^\infty W_p \frac{\partial J_0(mr)}{\partial r}\,dm = M\int_0^\infty W_p[-mJ_1(mr)]\,dm \tag{18a}$$

$$\frac{\partial A_{zp}}{\partial z} = M\int_0^\infty \frac{\partial W_p}{\partial z} J_0(mr)\,dm = M\int_0^\infty a_p(g_p e^{a_p z} - b_p e^{-a_p z})J_0(mr)\,dm \tag{18b}$$

$$\frac{\partial^2 A_{zp}}{\partial z^2} = M\int_0^\infty a_p^2 W_p J_0(mr)\,dm. \tag{18c}$$

Making use of these results, the field-strength components can be computed in an arbitrary layer by the formulae:

$$H_p = \frac{I_z\,dl}{4\pi}\int_0^\infty [g_p e^{a_p z} + b_p e^{-a_p z}]m\,J_1(mr)\,dm, \tag{19}$$

$$E_{rp} = \frac{I_z\,dl}{\sigma_p 4\pi}\int_0^\infty a_p[b_p e^{-a_p z} - g_p e^{a_p z}]m\,J_1(mr)\,dm, \tag{20}$$

$$E_{zp} = \frac{I_z\,dl}{\sigma_p 4\pi}\int_0^\infty (-k_p^2 + a_p^2)[g_p e^{a_p z} + b_p e^{-a_p z}]\,J_0(mr)\,dm. \tag{21}$$

If the source is situated at $z=-0$, we have $-2m/k_1^{*2}$ on the right-hand side of Eq. (10), that is, in Eqs. (12)–(15) m/k_1^{*2} should be written in the numerator instead of m/k_1^2.

If $\sigma_1=\sigma_1^*$ the two dipole arrangements lead to identical computational results. If $\sigma_1\neq\sigma_1^*$, the field characteristics at a given point are computed by superimposing the values defined by the dipoles placed at $z=+0$ and $z=-0$, respectively.

3. The three-layer case

Let us now apply the theoretical results for the simplified case of practical importance, where an infinite space is divided into 3 parts by 2 horizontal boundaries *(Fig. 2)*. The dipole is placed at the centre of the intermediate layer of thickness H. The $z=0$ plane is only a fictitious layer boundary, that is $\sigma_1=\sigma_1^*$. Assume further that $\sigma_2=\sigma_2^*$, which implies the equality of the wavenumbers $k_1=k_1^*$ and $k_2=k_2^*$ and, on the strength of Eq. (6), of the exponents $a_1=a_1^*$; $a_2=a_2^*$. In the numerator in Eqs. (12)–(15) we shall have m/k_1^2.

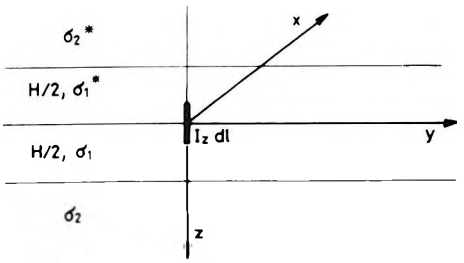

Fig. 2. Vertical electric elementary dipole placed at the centre of a bed bounded by infinitely extended underlying and overlying layers

2. ábra. A végtelen kiterjedésű fedővel és feküvel határolt telep közepén elhelyezett vertikális elektromos elemi dipólus

Рис. 2. Вертикальный элементарный электрический диполь, помещенный в центр залежи, ограниченной бесконечными кровлей и почвой

According to Eq. (9) the R_1 factor, describing the effect of layering, becomes:

$$R_1 = \operatorname{cotanh}\left(a_1\frac{H}{2}+\operatorname{ar\,cotanh}\frac{a_1\sigma_2}{a_2\sigma_1}\right), \tag{22}$$

Because of the geometrical symmetries, $R_1 = R_1^*$, the coefficients belonging to the central layer simplify to

$$b_1 = g_1^* = \frac{m}{2a_1}(R_1 + 1) \tag{23}$$

$$g_1 = b_1^* = \frac{m}{2a_1}(R_1 - 1) \tag{24}$$

which, of course, is quite natural since in this layer the field-strength components can be computed from a single vector potential.

Thus, in the central layer the electromagnetic field components become

$$H_1 = \frac{I_z\,dl}{4\pi}\int_0^\infty [g_1 e^{a_1 z} + b_1 e^{-a_1 z}] m J_1(mr)\,\mathrm{d}m \tag{25}$$

$$E_{r1} = \frac{I_z\,dl}{\sigma_1 4\pi}\int_0^\infty a_1 [b_1 e^{-a_1 z} - g_1 e^{a_1 z}] m J_1(mr)\,\mathrm{d}m \tag{26}$$

$$E_{z1} = \frac{I_z\,dl}{\sigma_1 4\pi}\int_0^\infty (-k_1^2 + a_1^2)\,[g_1 e^{a_1 z} + b_1 e^{-a_1 z}] J_0(mr)\,\mathrm{d}m \tag{27}$$

In order to show the conditions occurring in Hungarian coal prospecting, we carried out computations using Eq. (27) (with the parameters: $\varrho_1 = 200\ \Omega$m, $\varrho_2 = 20\ \Omega$m, $H = 2$ m, $r = 25$ m, i.e. in the near zone, and choosing $I_z\,dl = 1$ Am), for determining the vertical component of the electric field-strength within the coal seam, due to a vertical electric dipole inside the same seam. The integral of complex arguments figuring in Eq. (27) was approximated by a numerical quadrature fitted to the half-periods of the Bessel function. *Figure 3* shows the behaviour of Re E_z, Im E_z, $|E_z|$ and φ_{E_z}, in the equatorial plane of the transmitter dipole, from audio-frequencies up to middle-wavelength radio-frequencies. As for its general trend, the field behaves similarly as in a homogeneous space; the layering, however, affects the course of the curves. In the low-frequency range — up to about $\sqrt{T} = 0.05$ — the field-strength is mainly determined by Re E_z, that is, E_z is close to that measured by direct current. The Im E_z component shows a more capricious behaviour, its relative extrema and roots show the influence of the layering parameters. Between 0.05 and 0.005, $\sqrt{T}$ barely affects E_z, it mainly varies as a function of Re E_z ($\sqrt{T}$). For higher frequencies the significance of Im E_z also increases, that is, besides the Im E_z component Re E_z also changes rapidly. There appear changes of sign and relative maxima, which might have a role in interpretation; moreover, as a joint effect of the two components, E_z significantly decreases. The change of sign of

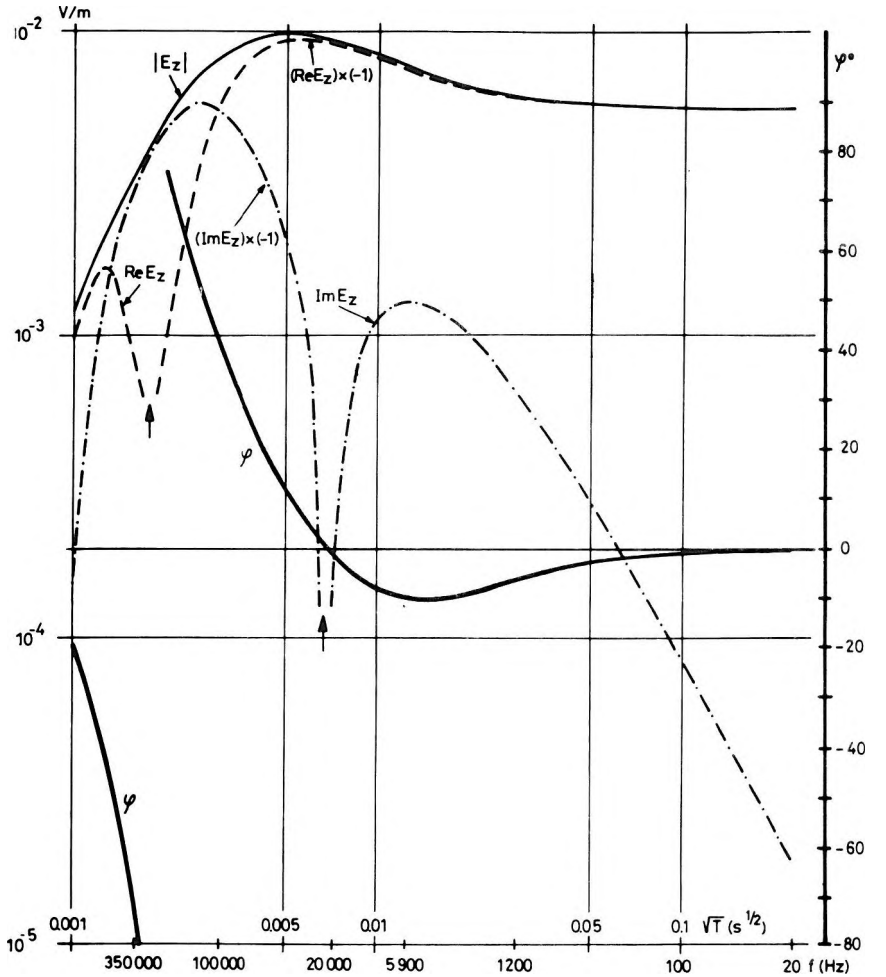

Fig. 3. Electric field-strength components of a vertical elementary dipole placed inside the seam. (Equatorial plane, $r = 25$ m, $H = 2$ m, $\varrho_1 = 200\ \Omega$m, $\varrho_2 = 20\ \Omega$m). ↑– change of sign

3. ábra. A telepben elhelyezett vertikális elemi dipólus vertikális elektromos térerősségének összetevői az ekvatoriális síkban ($r = 25$ m, $H = 2$ m, $\varrho_1 = 200\ \Omega$m, $\varrho_2 = 20\ \Omega$m). ↑– előjelváltás

Рис. 3. Компоненты вертикальной напряженности электрического поля вертикального элементарного диполя, помещенного в залежь, в экваториальной плоскости ($r = 25$ м, $H = 2$ м, $\varrho_1 = 200\ \Omega$м, $\varrho_2 = 20\ \Omega$м). ↑– перемена знака

the phase-angle curve also occurs in this range. The nature of the behaviour of the electromagnetic field is qualitatively illustrated in *Fig. 4* [after CORSON and LORRAIN 1962], showing force lines of the electric field at different time instants. The obvious lesson from this figure is that if one measures the field due to a dipole, placed in a seam, inside a gallery within the same seam, the electric properties of the bedrock and of the roof, respectively, do have a definite role with regard to the value of field strength.

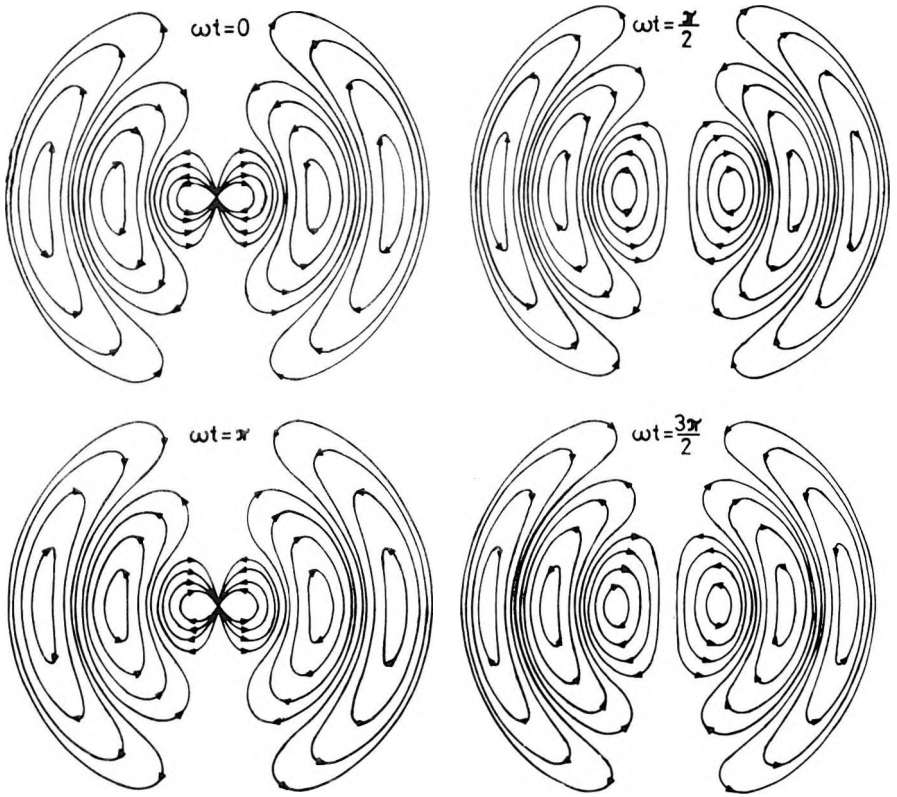

Fig. 4. Force lines of the electric field strength of an ac electric dipole for the time instants $\omega t = 0,\ \pi/2,\ \pi$ and $3\pi/2$

4. ábra. A váltóáramú elektromos dipólus elektromos térerősségének erővonalai az $\omega t = 0,\ \pi/2,\ \pi,\ 3\pi/2$ időpillanatokra

Рис. 4. Силовые линии электрической напряженности переменного электрического диполя в момент времени $\omega t = 0,\ \pi/2,\ \pi,\ 3\pi/2$

4. Effect of layering

In order to study the effect of layering, let us look at *Figs. 5–7,* showing the behaviour of the well-known apparent resistivity

$$\varrho_\omega = \frac{4\pi \cdot r^3 \, |E_z|}{I_z \, dl}$$

for different distances, r and layer thicknesses, H. For comparison, the frequency sounding curve belonging to a homogeneous space of the same resistivity as the seam is also indicated. The properties of the overlying and underly-

ing layers, respectively, can drastically change the position of the curves if a lower-resistivity rock-mass is placed in the way of the current systems of Fig. 4. If a greater current density comes into being, it creates a greater field strength. Correspondingly, for the investigated model, one can get apparent resistivities which are by an order of magnitude higher than the real resistivity. Thus, for such cases, the conventional definition of apparent resistivities used in surface geoelectrics, does not hold for in-seam measurements. As an effect of the layering assumed in the present model, the characteristic maxima ($\varrho_\omega^{(max)}$) of the curves are shifted to lower frequencies: the less thick the layer, the larger becomes this shift. Upon decreasing the thickness of the seam the total resistivity of the formation which has an effect on the distribution of the electromagnetic field becomes less and less, compared with the resistivity of the homogeneous model, and the maxima occur at lower frequencies.

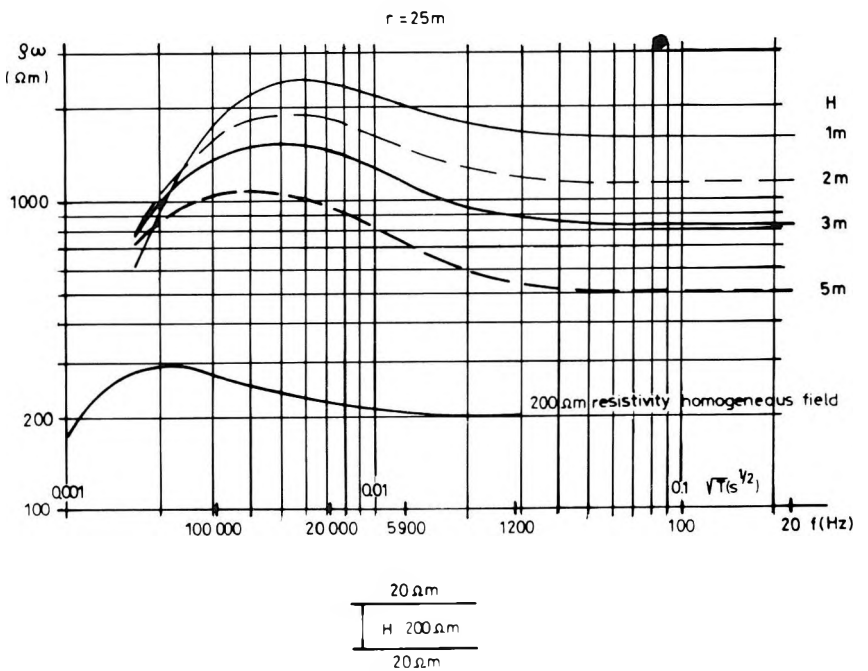

Fig. 5. Apparent resistivity curves ϱ_{t_ω} measured inside the seam, for $r = 25$ m, $\varrho_1 = 200$ Ωm, $\varrho_2 = 20$ Ωm, H = variable

5. ábra. A telepben mért ϱ_{t_ω} látszólagos fajlagos ellenállás görbék az $r = 25$ m, $\varrho_1 = 200$ Ωm, $\varrho_2 = 20$ Ωm, H = változó esetre

Рис. 5. Кривые кажущегося удельного сопротивления ϱ_{t_ω}, замеренные при $r = 25$м, $\varrho_1 = 200$ Ωм, $\varrho_2 = 20$ Ωм и H = переменная величина

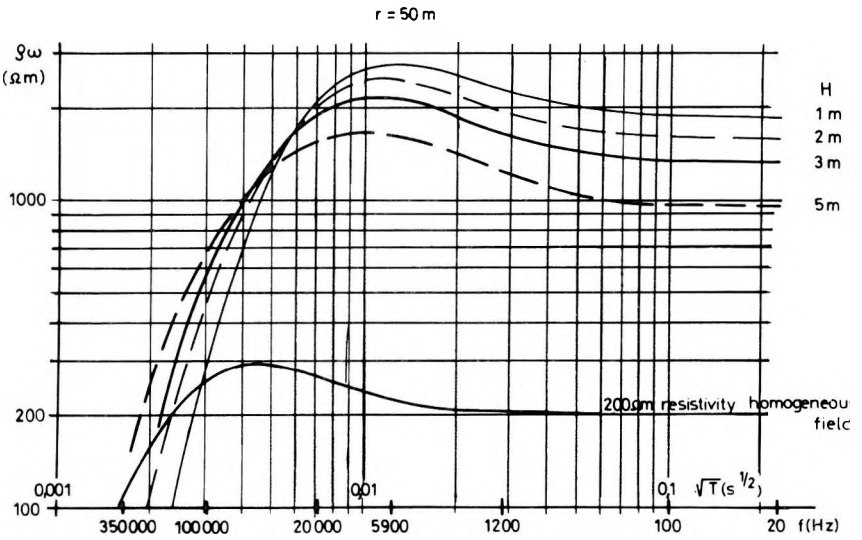

Fig. 6. Apparent resistivity curves ϱ_ω measured inside the seam, for $r = 50$ m, $\varrho_1 = 200\ \Omega$m, $\varrho_2 = 20\ \Omega$m, $H =$ variable

6. ábra. A telepben mért ϱ_ω látszólagos fajlagos ellenállás görbék az $r = 50$ m, $\varrho_1 = 200\ \Omega$m, $\varrho_2 = 20\ \Omega$m, $H =$ változó esetre

Рис. 6. Кривые кажущегося удельного сопротивления ϱ_ω, замеренные при $r = 50$ м, $\varrho_1 = 200\ \Omega$м, $\varrho_2 = 20\ \Omega$м и $H =$ переменная величина

For the case $r = 50$ m we also investigated the effects due to changes in the resistivity of the embedding rocks (ϱ_2) and in the resistivity of the seam (ϱ_1) — all other parameters being kept unchanged *(Fig. 8)*. As expected, a decrease in the resistivity of the host rock increases the value of the vertical electric field strength inside the seam, in the equatorial plane of the dipole. At the same time, because of the decreased "resultant" resistivity of the formation, the place of $\varrho_\omega^{(max)}$ is shifted towards lower frequencies. On the other hand, the decrease of

the resistivity of the seam leads to a decrease in the vertical component of the electric field strength, and $\varrho_\omega^{(max)}$ is shifted again toward lower frequencies. As for the shape of the curves, the deviation from the curves belonging to the homogeneous field becomes significant for higher ϱ_1 values, and lower ϱ_2 values, respectively. For given layer thicknesses the shape of the curves depends only on the ϱ_2/ϱ_1 ratio. For example, the curves in Fig. 8, corresponding to the set of parameters: $\varrho_2 = 10\ \Omega$m, $\varrho_1 = 200\ \Omega$m; and to $\varrho_1 = 400\ \Omega$m, $\varrho_2 = 20\ \Omega$m; or to $\varrho_2 = 40\ \Omega$m, $\varrho_1 = 200\ \Omega$m; $\varrho_1 = 100\ \Omega$m, $\varrho_2 = 20\ \Omega$m, respectively, are of identical shape, they are shifted only with respect to each other.

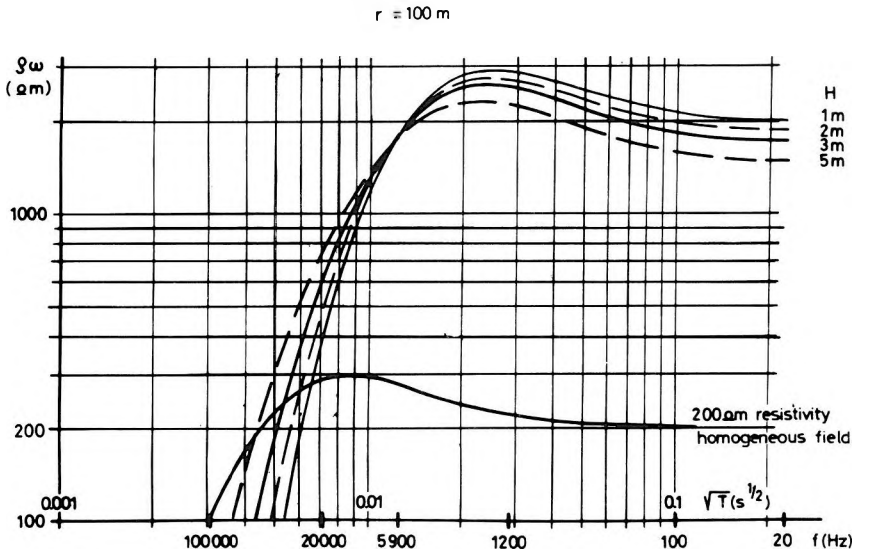

Fig. 7. Apparent resistivity curves ϱ_ω measured inside the seam, for $r = 100$ m, $\varrho_1 = 200\ \Omega$m, $\varrho_2 = 20\ \Omega$m, $H =$ variable

7. ábra. A telepben mért ϱ_ω látszólagos fajlagos ellenállás görbék az $r = 100$ m, $\varrho_1 = 200\ \Omega$m, $\varrho_2 = 20\ \Omega$m, $H =$ változó esetre

Рис. 7. Кривые кажущегося удельного сопротивления ϱ_ω, замеренные при $r = 100$ м, $\varrho_1 = 200\ \Omega$м, $\varrho_2 = 20\ \Omega$м и $H =$ переменная величина

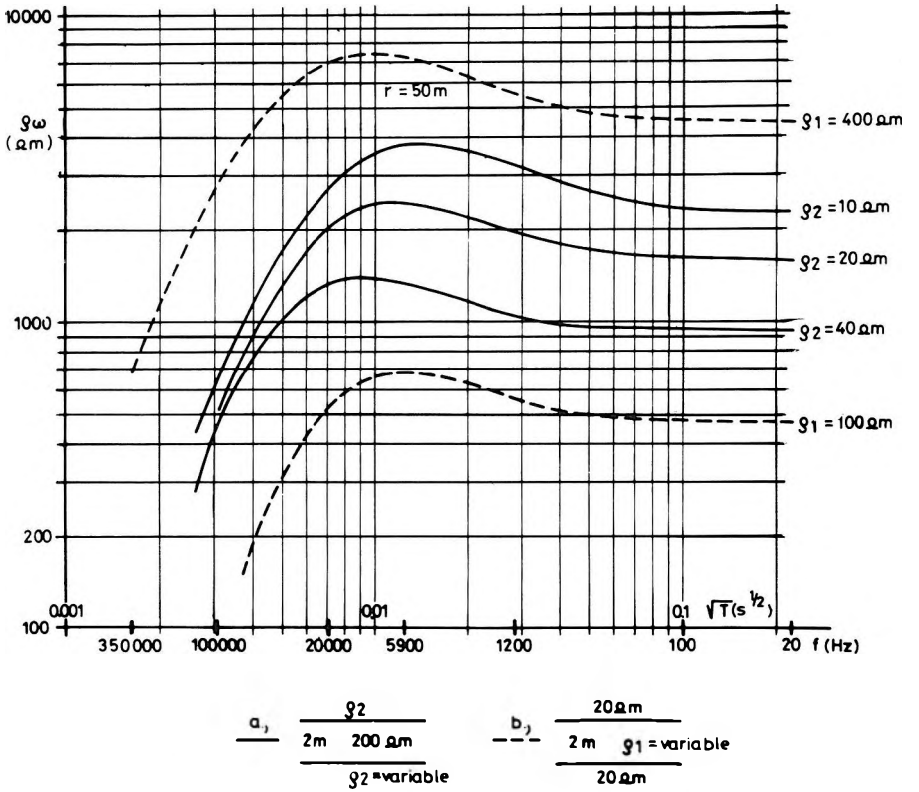

Fig. 8. Apparent resistivity curves ϱ_ω measured inside the seam, for $r = 50$ m, $H = 2$ m
a) $\varrho_1 = 200$ Ωm, $\varrho_2 =$ variable;
b) $\varrho_1 =$ variable, $\varrho_2 = 20$ Ωm

8. ábra. A telepben mért ϱ_ω látszólagos fajlagos ellenállás görbék $r = 50$ m, $H = 2$ m mellett az
a) $\varrho_1 = 200$ Ωm, $\varrho_2 =$ változó; és a
b) $\varrho_1 =$ változó, $\varrho_2 = 20$ Ωm esetekre

Рис. 8. Кривые кажущегося удельного сопротивления ϱ_ω, замеренные при $r = 50$ м и $H = 2$ м для случаев:
a) $\varrho_1 = 200$ Ωм, $\varrho_2 =$ переменная величина
b) $\varrho_1 =$ переменная величина, $\varrho_2 = 20$ Ωм

REFERENCES

CORSON, D., LORRAIN P. 1962: Introduction to electromagnetic fields and waves. W. H. Freeman and Co.

KAUFMAN A. A. 1974: Basic theory of inductive mineral prospecting (in Russian). Nauka, Novosibirsk, 350 p.

TAKÁCS E. 1979: Some application possibilities of electromagnetic methods in mining geophysics (in Hungarian). Magyar Geofizika **20**, 5, pp. 192–198

RÉTEGZETT KÖZEGBEN LEVŐ, VERTIKÁLIS, VÁLTÓÁRAMÚ, ELEKTROMOS ELEMI DIPÓLUS TERE

TAKÁCS Ernő, NAGY Jenő és MÁDAI Ferenc

A dolgozatban a szerzők levezetik a rétegzett térben levő, vertikális, váltóáramú elektromos elemi dipólus térerősség komponenseinek képleteit, a tetszőleges rétegben levő mérési helyre. E képletek felhasználásával konkrét térerősség- és látszólagos fajlagos ellenállás görbéket számítanak a dipól ekvatoriális síkjában mérhető vertikális elektromos összetevőt illetően homogén, végtelen kiterjedésű fedő és fekü között.

ПОЛЕ ВЕРТИКАЛЬНОГО ЭЛЕМЕНТАРНОГО ПЕРЕМЕННОГО ЭЛЕКТРИЧЕСКОГО ДИПОЛЯ, НАХОДЯЩЕГОСЯ В СЛОИСТОЙ СРЕДЕ

Эрнё ТАКАЧ, Йенё НАДЬ и Ференц МАДАИ

В работе выводятся формулы, описывающие компоненты напряженности вертикального элементарного переменного электрического диполя, находящегося в слоистой среде. С помощью этих формул производится расчет кривых напряженности и кажущихся удельных сопротивлений для вертикальной электрической компоненты, измеряемой в экваториальной плоскости диполя, находящегося между однородными и бесконечными кровлей и почвой.

GEOPHYSICAL TRANSACTIONS 1986
Vol. 32. No. 1. pp. 57–67

DETERMINATION OF FILTRATION COEFFICIENT OF WATER-BEARING SAND LAYERS BY WELL LOGGING

János CSÓKÁS*

Darcy's law for fluid filtration and Kozeny's relationship for permeability are of a similar form. Utilizing this similarity a functional relationship can be derived for well-sorted water-bearing sands, connecting the coefficient of tortuosity and the specific grain surface (i.e. filtration path) with Kozeny's effective grain diameter and the average shape factor of the grains (grain geometry). The coefficient of tortuosity and Kozeny's effective grain diameter can be determined from resistivity- and porosity logs, the specific surface can also be found if the effective grain diameter is known. The kinematic viscosity of pore water can be computed from layer temperature, obtained from the temperature log. Substituting these data into Darcy's law, the filtration coefficient can be determined with a fair approximation. The formulae derived in the present paper are especially recommended for investigations of water-bearing layers within coal seams, with the aim of protection against water inrush.

Keywords: filtration coefficient, specific surface, tortuosity, permeability

1. Introduction

Between the hanging- and footwalls of coal-bearing formations one frequently finds such water-bearing clastic sediments, shaly or pure sands, sandstones, gravels or pyroclastics which must be opened up and drained by means of boreholes, either from the surface or from the mine galleries, for the sake of protections against flooding. The water yield of such formations can be determined from their so-called Darcy filtration coefficient, or k-factor. The k-factor of porous water-bearing layers is determined from the temporal changes of the water level created by means of drainage or absorption in a well (or several wells) drilled into the given layer, the amount of water yielded by pumping tests, as well as from data of the monitoring wells. This way of determining the k-factor, however, is time-consuming and, for several reasons, inaccurate.

The above-described way to determine the k-factor is rarely possible in mines because of technical difficulties. On the other hand, geophysical well logging in exploratory boreholes penetrating the given water-bearing layer provides a continuous record of the variation of certain geophysical quantities, which are directly related to the k-factor. For logging purposes sondes of small diameter are available, which can be used even in holes of 60 mm diameter. The movement of the probes in the drill holes and the recording of the measured data are performed in the mines by portable devices.

* Department of Geophysics, Technical University for Heavy Industry, Miskolc, Egyetemváros, H–3515, Hungary

Manuscript received (revised form): 16 September, 1985

The technique to be described is most advantageous for hydrogeologic and stratigraphic studies of water-bearing layers of coal measures with several coal seams, where the deeper coal beds are explored by drilling from the above-lying mines.

2. Relationship between filtration path and grain geometry

The filtration coefficient of sands and sandstones consisting of mixed-grains can be expressed in terms of the properties of pore-water and rock matrix, according to Darcy's law, as

$$k = \frac{1}{5}\,\frac{\gamma}{\eta}\,\frac{n^3}{(1-n)^2}\left(\frac{D_h}{\bar{\alpha}}\right)^2 \tag{1}$$

where γ is the specific weight of the pore water, η is its dynamic viscosity, n the void ratio (porosity) of the rock, D_h the effective grain diameter introduced by Kozeny, and $\bar{\alpha}$ the average shape factor of the grains [Kovács 1981]. In porous rocks the flow of water depends on four factors: (i) the first of these is connected with the geometrical characteristics of the grains (grain shape, grain size, grain size distribution); (ii) the second with such rock properties as compaction, cementation and tortuosity. These characteristics are in connection neither with the fluid properties affecting the flow (specific weight and viscosity) nor with the type of motion of the fluid (laminary and turbulent flows). The properties depending on the rock can be contracted into a single factor K, which is termed permeability, viz.

$$K = \frac{1}{5}\,\frac{n^3}{(1-n)^2}\,\frac{D_h}{\bar{\alpha}}; \tag{2}$$

(iii) the third factor affecting water flow is the ratio describing the fluid properties. For this we have

$$\frac{\gamma}{\eta} = \frac{g}{\nu} \tag{3}$$

where $g = 9.81\ \mathrm{ms}^{-2}$ is the gravitational acceleration, ν is the kinematic viscosity of water, related to layer temperature, T (°C) as

$$\nu = \frac{1.778 \cdot 10^{-2}}{1 + 0.0337T + 0.000221T^2} \quad [\mathrm{m^2 s^{-1}}]; \tag{4}$$

(iv) the fourth — generally neglectable — factor expresses the dependence on pressure and salinity. Summing up, the factor describing fluid properties becomes

$$\frac{g}{\nu} = \frac{9.81(1 + 3.37 \cdot 10^{-2}T + 2.21 \cdot 10^{-4}T^2)}{1.778 \cdot 10^{-2}} = 551.74\,C \quad [m^{-1}s^{-1}] \tag{5}$$

where C denotes the temperature factor inside the brackets. Making use of Kozeny's equation, Eq. (2) can be rewritten so as to express the permeability of rock in terms of compaction, $n^3/(1-n)^2$, tortuosity coefficient, t and specific surface of mineral grain constituents S_v:

$$K = \frac{1}{5}\frac{n^3}{(1-n)^2}\left(\frac{1}{tS_v}\right)^2 \tag{6}$$

[PIRSON 1963]. For a bundle of capillary tubes the numerical factor is 1/2, for real rocks, however, an empirical factor of 1/5 has been found [CARMAN 1956].

By Eqs. (2) and (6) we can relate the coefficient of tortuosity and the specific grain surface, that is the filtration path, to Kozeny's effective grain diameter and the average grain shape factor, that is, to the grain geometry:

$$\frac{1}{tS_v} = \frac{D_h}{\bar{\alpha}} \tag{7}$$

Since porosity, tortuosity and specific grain surface can be determined by geophysical well logging, the permeability as well as the filtration coefficient, k can be determined by means of Eqs. (6) and (1).

3. Determination of the factors affecting permeability

Determination of the porosity

The porosity n can be determined with the required accuracy either from individual porosity logs (density-, neutron-, or acoustic logs) or from their combinations.

If we have resistivity logs only, we cannot compute the real porosity by means of the formation factor, as Archie's formula or its modified forms do not suffice in themselves to solve this problem in the case of fresh-water-bearing porous formations.

Determination of the tortuosity coefficient

For a model of a bundle of capillary tubes the tortuosity coefficient is $t^2 = Fn$ [PIRSON 1963]. Real rock however, has proved to be better approximated by the relation

$$t^{1.67} = Fn \tag{8}$$

[Ogbe–Bassiouni 1978], where

$$F = \frac{R_0}{R_w} \tag{9}$$

is the formation factor [Pirson 1963]. R_0 denotes the electric resistivity of the rock saturated by formation water, R_w that of the formation water, in situ. By Eqs. (8) and (9) the tortuosity coefficient can be expressed in terms of well-log data as

$$t = \left(\frac{R_0}{R_w} n\right)^{0.6} \tag{10}$$

Determination of the specific surface

The specific surface of a homogeneously dispersed system of spheres is

$$S_v = \frac{6}{D_h} \tag{11}$$

[cf. Pirson 1963]. In filtration calculations it is recommended that Kozeny's effective grain diameter be utilized since this takes into account grain size as well as its distribution [Kozeny 1953]. The effective grain diameter is defined as the diameter of spheres in a homogeneously dispersed system of spheres built up of identical diameter and density spheres in such a manner that the whole system has the same surface as the actual one.

Determination of Kozeny's effective grain-size diameter

In order to determine the effective grain-size diameter from well-log data, one should use several empirical formulae. In essence, these relationships serve as a substitute for the grain-size distribution histogram. If the grain-size distribution can be approximated by a mathematically easily describable curve then a relationship can be established between the characteristic grain diameters, which would also involve the "inequality factor" U [cf. Kovács 1981]. For the grain-size distribution of sand, the inequality factor U is defined as

$$U = \frac{D_{60}}{D_{10}} \tag{12}$$

where D_{60} denotes the grain diameter belonging to 60% on the grain-size distribution curve, while the value D_{10} corresponding to 10% is the so-called Hazen's standard grain diameter. For well-sorted water-bearing sands we usually have $2.0 \leqq U \leqq 2.5$ [Alger 1971].

For different kinds of sand the ratio of their characteristic grain-diameters is related to the logarithm of the inequality factor by

$$\frac{D_h}{D_{10}} = 1.919 \log U + 1.0 \tag{13}$$

in the above-mentioned range of U (see *Fig. 1.*), where D_h is the effective Kozeny grain size. If U changes between 2.0 and 2.5, the values of log U will range between 0.301 and 0.398, that is, on the average, the right-hand-side of Eq. (13) will be 1.671. Taking the mean value, the error is negligibly small, ± 0.093; that is, for fairly well-sorted fresh-water-bearing sands the effective Kozeny grain size is approximately related to the standard grain diameter of Hazen as

$$D_h = 1.671 \cdot D_{10} \tag{14}$$

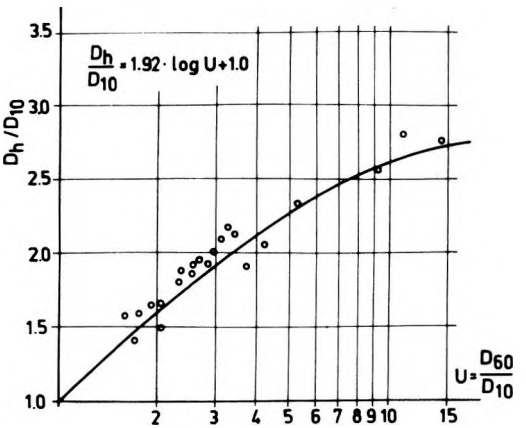

Fig. 1. Ratio of characteristic grain diameters for sand, as a function of the inequality factor [after Kovács 1981]

1. ábra. Homokok jellemző szemcseátmérő hányadosa az egyenlőtlenségi együtthatójuk függvényében [Kovács 1981 nyomán]

Рис. 1. Характерные отношения диаметров зерен в песках как функции коэффициента неравномерности [по Kovács 1981]

Taking the mean value of the two empirical formulae proposed by ALGER [1971], in order to connect Hazen's standard grain diameter with the formation factor (cf. Eq. 9), we get

$$D_{10}[\mathrm{m}] = 5.22 \cdot 10^{-4} \log \frac{R_0}{R_w} \tag{15}$$

presented in *Fig. 2.* From Eqs. (14) and (15) the effective grain diameter becomes

$$D_h[\mathrm{m}] = 8.723 \cdot 10^{-4} \log \frac{R_0}{R_w} \tag{16}$$

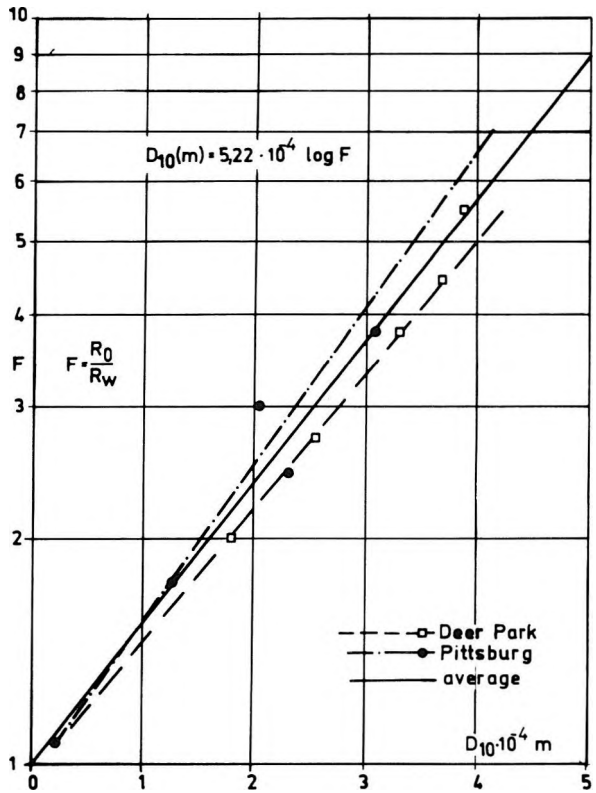

Fig. 2. Formation factor as a function of Hazen's standard grain diameter [after ALGER 1971]

2. ábra. A Hazen-féle mértékadó szemcseátmérő és a formációtényező összefüggése [ALGER 1971 nyomán]

Рис. 2. Зависимость формационного фактора от стандартного диаметра зерен по Хазену [по ALGER 1971]

That is, upon substituting Eq. (16) into (11), the specific surface becomes

$$S_v\left[\frac{\mathrm{m}^2}{\mathrm{m}^3}\right] = \frac{6}{8.723 \cdot 10^{-4} \log \dfrac{R_0}{R_w}} \tag{17}$$

If we substitute Eqs. (10) and (17) into (6) and carry out numerical operations, we obtain the following expression for permeability:

$$K[\mathrm{m}^2] = 4.227 \cdot 10^{-9} \frac{n^3}{(1-n)^2} \frac{\left(\log \frac{R_0}{R_w}\right)^2}{\left(\frac{R_0}{R_w} n\right)^{1.2}} \tag{18}$$

(Let us recall here that $10^{-9}\ \mathrm{m}^2 = 10^3$ darcy).

If the rock is poorly sorted ($U \gg 2.5$) and/or it contains a significant amount of flat grains ($\bar{\alpha} \gg 9$), the coefficient figuring in Eq. (18) should be modified empirically so as to give a more accurate value of the filtration coefficient.

4. Equation for the filtration coefficient

Upon multiplying Eq. (18), describing permeability, by the factor describing the temperature-dependence of the kinematic viscosity of the filtrating water (Eq. 5), an equation is obtained for the filtration coefficient, k:

$$k[\mathrm{ms}^{-1}] = 2.332 \cdot 10^{-6}\, C \frac{n^3}{(1-n)^2} \frac{\left(\log \frac{R_0}{R_w}\right)^2}{\left(\frac{R_0}{R_w} n\right)^{1.2}} \tag{19}$$

The coefficient C, as a function of temperature, can be read off the curve of *Fig. 3.*

If the assumptions made on grain-size distribution and grain shape are poorly met, the coefficient of Eq. (19) should be corrected on the basis of the grain-size distribution curve or by means of another log (gamma-ray) to achieve a better fit with permeability.

5. A case history

ALGER [1971], describes a study where the relations between grain-size, formation factor and permeability were investigated on nine sand samples taken from water wells. The standard grain diameters, D_{10} were determined from the grain-size distribution curves of the samples; the R_0 resistivities of the samples were measured for pore waters of three different resistivities; the porosities and the formation factors belonging to the three different pore-fluids were determined. These data, as well as the values of permeability and of the filtration coefficient are compiled in *Table I.*

On the basis of this table, the following conclusions can be made:

1. For all samples the formation factor, F, the filtration coefficient, k, and the permeability K decrease with increasing resistivity, R_w of the saturant.

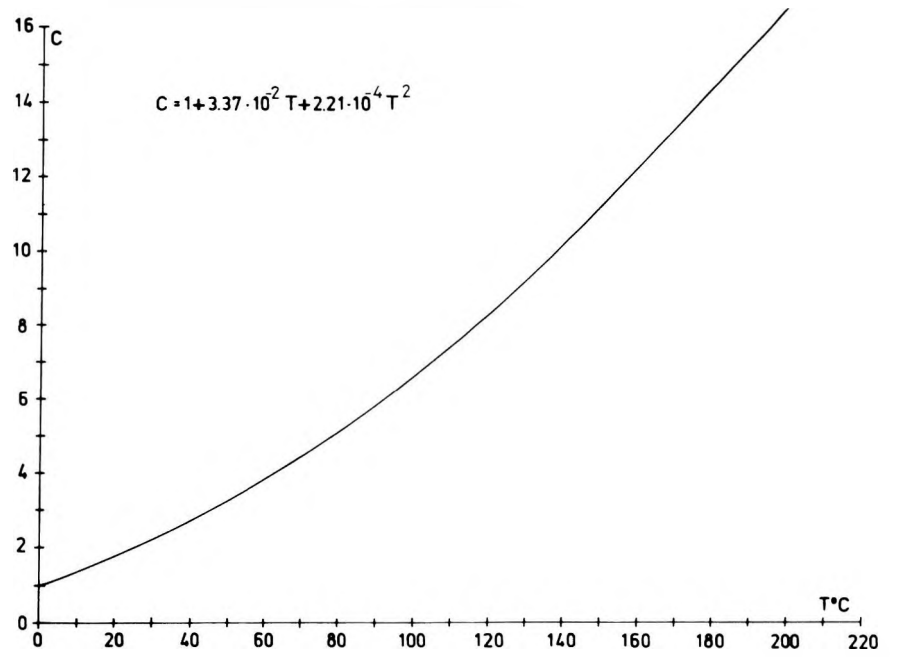

Fig. 3. Temperature factor of filtration coefficient

3. ábra. A szivárgási tényező hőmérsékleti együtthatója

Рис. 3. Температурный коэффициент фильтрационного фактора

2. When the samples were first saturated by brine of $R_w = 1.1\ \Omega$m resistivity ($5 \cdot 10^3$ ppm NaCl concentration at 25 °C), and subsequently by brine of 7.1 Ωm resistivity ($7 \cdot 10^2$ ppm), the filtration coefficient of the samples did not decrease more than a few per cent: $k(1.1) - k(7.1) = (2-6) \cdot 10^{-9}\ \mathrm{ms}^{-1}$.
3. The decrease of the filtration coefficient is by an order of magnitude larger if the samples are saturated by fresh water of 32.0 Ωm resistivity ($1.5 \cdot 10^2$ ppm):

$$k(1.1) - k(32.0) = (10-50) \cdot 10^{-9}\ \mathrm{ms}^{-1}$$
$$k(7.1) - k(32.0) = (\ 8-32) \cdot 10^{-9}\ \mathrm{ms}^{-1}.$$

4. The phenomenon is due to the fact that the resistivity, R_w of water was originally determined for the total mass of water. Rock resistivity R_0 was also accepted as a steady-state value, achieved after saturation and compaction. On the other hand, the resistivity, R_w belonging to the total mass of water has decreased because of ion exchange with the mineral grains, and because of dissociation, surface conductivity and adsorption. The less the original concentration of salt in the water saturating the samples, the larger would become this subsequent resistivity decrease.

No.	D_{10} [μm]	$n=\Phi$	R_w Ωm	$R_w^* = R_0/F$ $(R_w=1.1)$	R_0 Ωm	$F=\frac{R_0}{R_w}$	K darcy $[10^{-12}\ m^2]$	$k10^{-9}[ms^{-1}]$ $T=2,5\ °C,\ C=2.0$	k(1.1)–k(7.1)	k(7.1)–k(32)	k(1.1)–k(32)
1	76.2	0.375	1.1 7.1 32.0	— 17.6	4.30 — 68.50	3.90 — 2.14	126.3 — 81.1	139 — 89	—	— —	— 50
2	76.2	0.372	1.1 7.1 32.0	— 22.3	— 23.40 73.60	— 3.30 2.30	— 116.0 87.0	— 128 96	—	— 32	— —
3	76.2	0.375	1.1 7.1 32.0	— 20.4	4.30 — 79.40	3.90 — 2.48	126.3 — 96.9	139 — 107	—	— —	— 32
4	127.0	0.341	1.1 7.1 32.0	 6.5 21.7	4.73 27.75 93.50	4.30 3.91 2.92	97.8 95.8 88.4	108 106 98	2	 8 	 10
5	177.8	0.358	1.1 7.1 32.0	 6.3 22.0	4.84 27.82 96.60	4.40 3.92 3.02	112.9 110.3 98.7	125 122 109	3	 13 	 16
6	177.8	0.345	1.1 7.1 32.0	 6.2 20.4	4.92 27.82 91.30	4.47 3.92 2.85	101.7 99.1 85.4	112 109 94	3	 15 	 18
7	190.5	0.332	1.1 7.1 32.0	 6.2 —	5.16 29.10 —	4.70 4.10 —	91.8 89.9 —	105 99 —	6	 — 	 —
8	203.2	0.336	1.1 7.1 32.0	 6.5 20.9	5.16 30.40 98.30	4.70 4.27 3.07	94.9 93.7 83.1	105 103 92	2	 11 	 13
9	304.8	0.340	1.1 7.1 32.0	 6.0 —	5.50 29.80 —	5.00 4.20 —	98.6 96.6 —	109 107 —	2	 — 	 —

Table I. Relation between grain-size, formation factor and permeability [after ALGER 1971]
I. táblázat. A szemcsenagyság, a formáció faktor és a permeabilitás közötti összefüggés [ALGER 1971 után]
Таблица I. Соотношение между размером зерен, формационным фактором и проницаемостью [по ALGER 1971]

5. The ratio of the resistivity, R_0 of the samples to the resistivity, R_w measured in the total mass of water is not equal to the real formation factor of the rock, as the resistivity of water changes inside the pores of the rock.
6. According to Table I, the decrease of the filtration coefficient of the rock samples in only 2–3% in the case of saturation by water of 1.1 Ωm and 7.1 Ωm resistivity, respectively, even though their porosity is 33.2–35.8%, and their standard grain-size D_{10} lies in the 127.0–203.2 μm range.

The resistivity of 32.0 Ωm of the fresh water has decreased – using the formation factor F belonging to R_w = 1.1 Ωm – to 22.3–17.6 Ωm inside the pores, that is by some 30–45%. On the other hand, the 7.1 Ωm dropped only to 6.5–6.0 Ωm, i.e. it has become only 8.5–15.5 per cent less. If we substitute the real formation factors – computed from the R_w specific resistivities valid inside the pores – into Eqs. (18) and (19), the permeabilities and filtration factors, respectively, of the different rock samples will be the same, independently of the specific resistivities of pore water and of rock, respectively.

The use of Eqs. (18) and (19) is primarily recommended for the delineation of producing layers penetrated by water-prospecting boreholes and for determining the expectable water yield. Additionally, these equations can be used for designing the protection system against water inrush in coal mines, by determining the filtration coefficients of water bearing sandstones and by locating running sand layers.

REFERENCES

ALGER R. P. 1971: Interpretation of electric logs in fresh-water wells in unconsolidated formations. SPE Reprint Series No. 1. pp. 246–270

CARMAN P. C. 1956: Flow of gases through porous media. London. 182 p.

KOVÁCS GY. 1981: Seepage hydraulics. Akadémiai Kiadó, Budapest, 730 p.

KOZENY J. 1953: Hydraulik. Wien

OGBE D., BASSIOUNI Z. 1978: Estimation of aquifer permeabilities from electric well logs. The Log Analyst, **19**, 5, pp. 21–27

PIRSON S. I. 1963: Handbook of Well Log Analysis. Prentice-Hall, Inc. Englewood Cliffs, N. J.

VÍZTÁROLÓ HOMOKRÉTEGEK SZIVÁRGÁSI TÉNYEZŐJÉNEK MEGHATÁROZÁSA FÚRÓLYUKSZELVÉNYEZÉSSEL

CSÓKÁS János

A Darcy-féle szivárgási egyenlet és a Kozeny-féle permeabilitás formula hasonló. Ennek alapján jól osztályozott víztároló homokokra felírható a tortuozitási együttható és a fajlagos szemcsefelület (a szivárgási pálya), valamint a Kozeny-féle hatékony szemcseátmérő és a szemcsék átlagos alaki tényezője (a szemcse-geometria) közötti függvény. A tortuózitási tényezőt és a Kozeny-féle hatékony szemcseátmérőt a fajlagos ellenállás és a porozitás szelvényekből meg lehet határozni. A fajlagos felületet pedig a hatékony szemcseátmérő ismeretében lehet megadni. Hőmérséklet szelvényből kapott réteghőfok ismeretében a pórusvíz kinematikai viszkozitása számítható. A fent említett adatokat a Darcy-féle egyenletbe behelyettesítve a szivárgási tényezőt jó közelítéssel meg lehet kapni. A cikkben levezetett egyenletek főleg széntelepes összletek víztároló rétegeinek hidrológiai vizsgálatára javasolhatók a vízvédelem tervezéséhez.

ОПРЕДЕЛЕНИЕ КОЭФФИЦИЕНТА ФИЛЬТРАЦИИ ПЕСЧАНЫХ ВОДОНОСНЫХ КОМПЛЕКСОВ ПУТЕМ КАРОТАЖА БУРОВЫХ СКВАЖИН

Янош ЧОКАШ

Уравнение фильтрации Дарси сходна с формулой проницаемости Козени. На этом основании можно вывести формулу зависимости удельной поверхности зерен (траекторий фильтрации) с коэффициентом, характеризующим сложность поровых каналов, от эффективного диаметра зерен по Козени со средним параметром формы зерен (геометрии зерен). Коэффициент, характеризующий сложность поровых каналов, и эффективный диаметр зерен по Козени можно определить по кривым удельных сопротивлений и пористости, а удельную поверхность можно задать по известному эффективному диаметру. На основании известной температуры слоя, определенной по температурным кривым, можно рассчитать кинематическую вязкость поровых вод. Подставляя полученные данные в уравнение Дарси, можно с достаточной точностью определить коэффициент фильтрации. Уравнения, выведенные в настоящей работе, могут быть рекомендованы в первую очередь в гидрологических исследованиях водоносных горизонтов угленосных толщ.

GEOPHYSICAL TRANSACTIONS 1986
Vol. 31. No. 1. pp. 69–79

DETERMINATION OF HYDROCARBON SATURATION, ROCK COMPOSITION, POROSITY AND PERMEABILITY IN CLAYEY–SILTY SANDSTONES EXHIBITING SANDWICH-TYPE DEVELOPMENT

Zoltán BARLAI* and Ferenc RÉZ**

A new interpretation system for hydrocarbon-bearing sandstones (COMWELL–B. R./ELGI) has been developed based on an earlier theory. This theory has further been developed so that sandstones are treated as composed of 8 components, viz. 1) impermeable shale laminae in the sandwich-type sandstone, 2) swelling-type clays, 3) nonswelling clays, 4) silt, 5) sand, 6) carbonate, 7) porosity in the permeable thin laminae, 8) adsorption water porosity. The interpretation system is built up on a statistical basis in the framework of an overdetermined mathematical treatment of the unknown quantities. However, the system is of modular nature enabling it to be divided into deterministic subsystems. A sequential calibration possibility is provided by the subsystems.

The new technique for evaluating the hydrocarbon saturation involved in this system is of special interest since routine techniques frequently fail in sandwiches. Besides the theoretical and practical aspects, a field example is shown from an oil- and gas-reservoir.

Keywords: shaly sandstone model, anisotropic model, dispersed clay and silt, laminated clay and silt, lithologic influence factor

1. Introduction: Problem performance

Oil/gas-bearing sandstones in Hungary are of fine-grained clayey–silty (sometimes calcareous) development and frequently follow a laminated "sandwich-type" depositional pattern. Well-log interpretation difficulties associated with this kind of lithology are further increased by fresh water in the reservoirs. Under these conditions hydrocarbons may not be recognized by current routine interpretation techniques since the electric resistivity of the said formations is near to the resistivity of water-bearing clean sand.

Sharp resistivity reductions in pay zones are caused by three main effects [BARLAI 1969, 1972, 1974]:

1. Resistivity of the interlaminated shale streaks is only 1.3–2.0 Ωm whereas that of the water-bearing sand is 4–10 Ωm, consequently the longitudinal resistivity, R_L, of the laminated anisotropic formations will not be significantly higher than the resistivity of the shale if relative volume, p, of the latter is large ($p > 0.2$);

* Eötvös Loránd Geophysical Institute of Hungary, POB 35, Budapest, H–1440
** Interface Computer Co., Kiss József u. 4, Budapest, H–1081
Manuscript received: 22 July, 1985

2. Within the permeable sand laminae the electric conductance of the cationic adsorption water, covering the clay and silt grains, is high resulting in an additional resistivity reduction of the permeable interbeddings;
3. Irreducible water saturation is high ($S_{wi}=0.4$–0.6) in the clayey–silty sands because of the small pore sizes and the associated large specific surface area of the pores. The resistivity will be further reduced by the high irreducible water saturation.

Permeability performance of the said formations is also complex and shows great variations and often goes below the permeability cutoff, especially in calcareous sandstones since a part of narrow pore channels will be blocked by the carbonate.

A great deal of effort has led to some results being achieved in Hungary [Barlai 1969, 1972, 1974, 1976, 1981] in helping to solve well-log interpretation difficulties. The technique used has been incorporated in a computerized well-log interpretation system called COMWELL–B. R./ELGI. The following main constituents are involved in this system:

1. An anisotropic sandstone model of nine components;
2. Multicomponent response functions of the main well-logging parameters;
3. A comprehensive program package put on a hybrid basis of a great number of deterministic and statistical procedures of interpretation;
4. A special calibration system covering the total interpretation flow;
5. A special technique for evaluating water saturation in sandwiches (based on the concept of multiple comparison);
6. A variety of interpretation outputs covering volumetric rock components, porosity- and fluid saturation terms, hydraulic- and capillary properties, and a detailed delineation of the reservoir related to the probable recovery and production behaviour of the individual zones.

2. Anisotropic sandstone model of nine components

To cope with the said problems an anisotropic sandstone model of nine components has been developed. The model is composed of a fourfold shale, a threefold porosity system, and a double-component inert matrix, as shown in *Fig. 1*. The shale has been distributed into:

- impermeable shale laminae with a volumetric fraction p; thus the permeable interbeddings have a volumetric fraction $(1-p)$;
- disseminated clay, V_{cl}, within the permeable laminae; this component has further been divided into swelling and nonswelling clays: $V_{cl,\ sw}$ and $V_{cl,\ nsw}$, respectively:
- silt, V_{si}, also within the permeable interbeddings.

All these shale components are characterized by their own geophysical properties and they differ very much from each other. Consequently, any kind of merging/averaging might lead to serious misunderstanding of the logging parameters and misleading errors in their interpretation especially when saturation

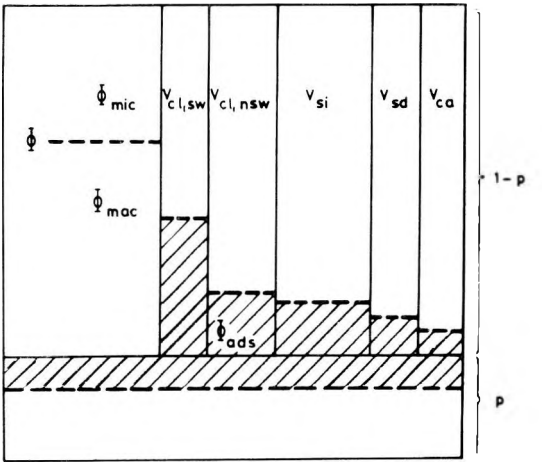

Fig. 1. Volumetric model of shaly sandstone. p — relative volume of impermeable shale laminae. Components of shale within the permeable laminae: $V_{cl,\,sw}$ — disseminated swelling clay, $V_{cl,\,nsw}$ — disseminated nonswelling clay, V_{si} — silt. Components of the matrix: V_{sd} — sand, V_{ca} — carbonate. The pore system in the permeable laminae: Φ — effective porosity (Φ_{mac} — effective macro porosity, Φ_{mic} — effective micro porosity), Φ_{ads} — porosity of adsorption water

1. ábra. Agyagos homokkő térfogati modellje. p — impermeábilis agyagmárga csíkok relatív térfogata. A permeábilis kőzetcsíkokon belüli agyag komponensek: $V_{cl,\,sw}$ — duzzadó agyag, $V_{cl,\,nsw}$ — nem duzzadó agyag, V_{si} — kőzetliszt. A mátrix komponensei: V_{sd} — homok, V_{ca} — karbonát. A pórusrendszer a permeábilis kőzetcsíkokban: Φ — effektív porozitás (Φ_{mac} — effektív makroporozitás, Φ_{mic} — effektív mikroporozitás), Φ_{ads} — adszorpciós porozitás

Рис. 1. Объемная модель глинистого песчаника. p — относительный объем прослоев непроницаемых глинистых мергелей. Глинистые компоненты в пределах проницаемых прослоев: $V_{cl,\,sw}$ — глины набухающие, $V_{cl,\,nsw}$ — глины ненабухающие, V_{si} — алевриты. Компоненты цемента: V_{sd} — пески, V_{ca} — карбонаты. Система пор в пределах проницаемых прослоев: Φ — эффективная пористость проницаемых прослоев (Φ_{mac} — эффективная макропористость проницаемых прослоев, Φ_{mic} — эффективная микропористость проницаемых прослоев), Φ_{ads} — адсорбционная пористость

is concerned. A similar tendency to distinguish the shale components can be seen with SARABAND [POUPON et al. 1970] and with CLASS [FERTL 1981].
The pore system has been divided into:
– effective porosity, Φ
– porosity of adsorption/hydration water, Φ_{ads}.
The effective porosity has further been distributed into:
– effective macro porosity, Φ_{mac},
– effective micro porosity, Φ_{mic}.
Φ_{mac} and Φ_{mic} are separated from each other by the size of the equivalent hydraulic radius of the pores: the bound between them is at $3 \cdot 10^{-4}$ cm. This kind of separation is of importance since high irreducible water saturations, low resistivities and low permeabilities will occur in high micro porosity even if the

total porosity of the rock is relatively high. The total porosity is the sum of the effective porosity and the hydration water porosity:

$$\Phi_t = \Phi + \Phi_{ads} = \Phi_{mac} + \Phi_{mic} + \Phi_{ads} \tag{1}$$

Finally the inert part of the rock matrix has been divided into:
- sand, V_{sd},
- carbonate, V_{ca},

since, if this were not done, porosity and permeability interpretations would fail in the case of calcareous sandstones.

3. Response functions of well logging parameters

At present seven logging parameters are incorporated in COMWELL-B.R./ELGI, viz:
- SP reduction factor, α
- gamma-ray intensity, I_{GR};
- bulk density, ϱ_b;
- neutron limestone porosity, Φ_{Nlm};
- acoustic propagation time of compressional waves, Δt;
- true resistivity of uncontaminated zone, R_t;
- flushed zone resistivity, R_{xo}.

Obviously the introduction of further advanced logging inputs (spectral gamma, acoustic shear waves, etc.) into the interpretation system is possible.

Response functions of logging parameters have been introduced to the system on a multicomponent basis corresponding to the 9-component sandstone model. With regard to the elucidation of the response functions, references [Barlai 1972, 1974, 1981] should be consulted. However, it is mentioned that with regard to the resistivity, R_t, of the sandstones the central role of accounting for the shale effects has been put in COMWELL-B. R./ELGI on the "lithologic influence factor", L, which is a ratio of the electric surface conductance, C_p, of the pores to the volume conductance C_Φ, of the effective pore space (when the latter is water-filled):

$$L = \frac{C_p}{C_\Phi}. \tag{2}$$

L comprises the individual effects of the rock components in the permeable isotropic interbeddings:

$$L = \left(\frac{V_{cl,\,sw}}{R_{cl,\,sw}} + \frac{V_{cl,\,nsw}}{R_{cl,\,nsw}} + \frac{V_{si}}{R_{si}} + \frac{V_{sd}}{R_{sd}} + \frac{V_{ca}}{R_{ca}} \right) \frac{R_w}{\Phi} \tag{3}$$

By analysing the correspondence with the SHELL [see for example JUHÁSZ 1981] and the Schlumberger dual-water [see for example BEST et al. 1978] models, we concluded that the formal analogous quantities of the said models – at least in water-bearing rocks – are:

$$L \sim BR_W Q_V \tag{4}$$

for the SHELL model,

$$L \sim S_{WB} \frac{R_{WF} - R_{WB}}{R_{WB}} \tag{5}$$

for the dual-water model. The meaning of the symbols is explained in references [JUHÁSZ 1981] and [BEST et al. 1978]

4. Hybrid interpretation system in COMWELL–B. R./ELGI: deterministic and statistical ways: system-calibration

The most complete form of geophysical interpretation has been offered by the statistical way [HOLTZMAN 1975; SALÁT et al. 1982; MAYER et al. 1981], since all available logging parameters can simultaneously be introduced into it in a weighted form, where the relative weights of the individual logging inputs, W_i, are determined by their reciprocal standard errors, $1/\sigma$. The system is mathematically "overdetermined" since the number of inputs is greater than that of the outputs, with the intention of reducing the production of errors in the outputs.

COMWELL–B. R./ELGI has been put on statistical basis, similarly to GLOBAL [MAYER et al. 1981], however the former is of hybrid nature since the deterministic way of interpretation has also been preserved in three forms:

1. Preliminary stage of interpretation is performed in it by deterministic subsystems, where the mathematical solution is "unique", i.e. the number of inputs is equal to those of outputs. In this way the mathematical treatment is more simple and fast – these features being important in the preliminary stage;
2. Deterministic subsystems follow each other in sequential form and only a small number of outputs are determined within one step. The individual steps can be self-calibrated and error propagation can be restricted in this way;
3. Calibration of the deterministic subsystems is easily performed by means of cross-plots; the first set of system-constants will then be determined.

The final calibration of the system-constants is still performed by statistical optimization. In doing so quadratic deviations of theoretical values of the logging parameters from the measured ones will be minimized for the total evaluated borehole section.

Error analyis is an important part of all statistical systems, thus also of COMWELL–B. R./ELGI. Instead of analytical derivation, the method of finite differences (i.e. the ratio of finite differences) is applied since it is very fast and

reliable. Random errors of corrections, response functions and interpretation outputs are estimated by the Gauss error propagation theorem. Systematic errors are diminished by statistical comparison of interpretation outputs with statistically representative core data.

A special system-logic is incorporated in COMWELL–B.R./ELGI, namely deterministic and statistical subsystems support each other in a hybrid form in order to arrive at the final convergence of the solutions with a good accuracy at a relatively low cost.

5. Determination of water saturation in sandwiches on the basis of comparison

The determination of the water saturation in sandwiches is an unsolved problem of log analysis [BARLAI 1967; VAJNAR et al. 1977; BOS 1982; ALLEN 1984] under the conditions when $R_p < R_0$. Here R_0 is the resistivity of the permeable laminae if they were water-filled; and R_p is the resistivity of the nonpermeable interbeddings. Since longitudinal resistivities of these formations are very low, movable hydrocarbon reserves in the permeable laminae often cannot be revealed at all.

COMWELL–B.R./ELGI introduced a special technique of comparison to evaluate the water saturation in sandwiches; a threefold comparison is applied:

1. Comparison of $(R_t)_s$ with $(R_{xo})_s$ where subscript s represents the permeable laminae;
2. Comparison of the theoretical log responses with the measured ones;
3. Comparing the logging properties at the investigated depth with the same properties of adequate reference layers, where the water saturation should be known with a fair accuracy from other information (e.g. the reference layer is water-bearing, thus $S_w = 1.0$).

In this way the effects of some systematic errors of the total logging and evaluating job will be reduced. Moreover R_w, R_{mf} and Φ will also be eliminated from the evaluation process. We are of the view that the evaluation of water saturation can appreciably be improved in this way, i.e. by combining the absolute and the comparative determinations.

6. Interpretation outputs determined by COMWELL–B.R./ELGI

Besides the evaluation of solid rock components (p; $V_{cl\,sw}$; $V_{cl\,nsw}$; V_{si}; V_{sd}; V_{ca}), porosity terms (Φ_{mac}, Φ_{mic}, Φ, Φ_{ads}, Φ_t) and saturation components (S_w, S_{wi}, S_{wm}; S_{hy}, S_{hyr}, S_{hym}) related to the effective porosity, the saturation terms are evaluated also–as related to the total porosity (S_{wt}, S_{hyt}, etc.).

As an example the formula for evaluating the adsorption/hydration water-filled porosity is shown here:

$$\Phi_{ads} = L\Phi \frac{R_{ads}}{R_w}, \tag{6}$$

where R_{ads} is the resistivity of the adsorption/hydration (i.e. "bound") water.

Permeability, k, is evaluated from a combination of the lithologic influence factor, L, and the effective porosity, Ω, through the hydraulic equation by Kozeny–Carman [Kozeny 1927; Carman 1956]. In addition, the specific surface area, S_p, of the rock can also be estimated [Barlai 1976].

Residual hydrocarbons, S_{hyr}, are determined from Φ/k on the basis of calibration with core data; for this purpose S_{hyr} is obtained from relative permeability measurements. S_{wi} is obtained from a combination of the lithologic influence factor and the porosity [Barlai 1974]. Some capillary properties can also be determined [Barlai et al. 1981], thus:

P_{displ} – capillary displacement pressure;

G – pore geometric factor;

$\bar{P}_c$ – a representative average capillary pressure of the pores, corresponding to the average hydraulic radius of the interconnected pores.

The capillary properties are related to each other by the following formula [Barlai 1981]:

$$\bar{P}_c = P_{displ} \cdot e^G \tag{7}$$

Last but not least, a detailed delineation of the reservoir regarding the possible recovery behaviour of the individual zones can be achieved by utilizing the variety of interpretation outputs [Barlai 1981]. This kind of delineation may contribute to production control of the reservoir especially when enhanced recovery technologies are concerned.

7. Field example utilizing COMWELL–B. R./ELGI

Outputs of application are presented in *Fig. 2* in borehole ALG-YO No. 809 of the Algyő field in Hungary. In *Fig. 2/a* the volumetric composition of the geological sequence, incorporating shaly sandstones and impermeable shales, is shown. In this case Φ, Φ_{mac}, Φ_{mic}, V_{sd}, V_{si}, p and V_{cl} as rock forming components have been taken into account in the interpretation model. It seems from the output plot that a great amount of V_{si}, p and V_{cl} are present in the shaly sand, and in a number of layers $\Phi_{mic} > \Phi_{mac}$ which is an indication of poor hydraulic properties.

In *Fig. 2/b* the permeability and fluid saturation plots are presented. The top section from 1835 m to 1878 m is water-bearing, the bottom section from 1880 m to 1937 m is oil-bearing. It seems that variations of permeability, k, correlate well with rock composition, the latter having been shown in Fig. 2/a.

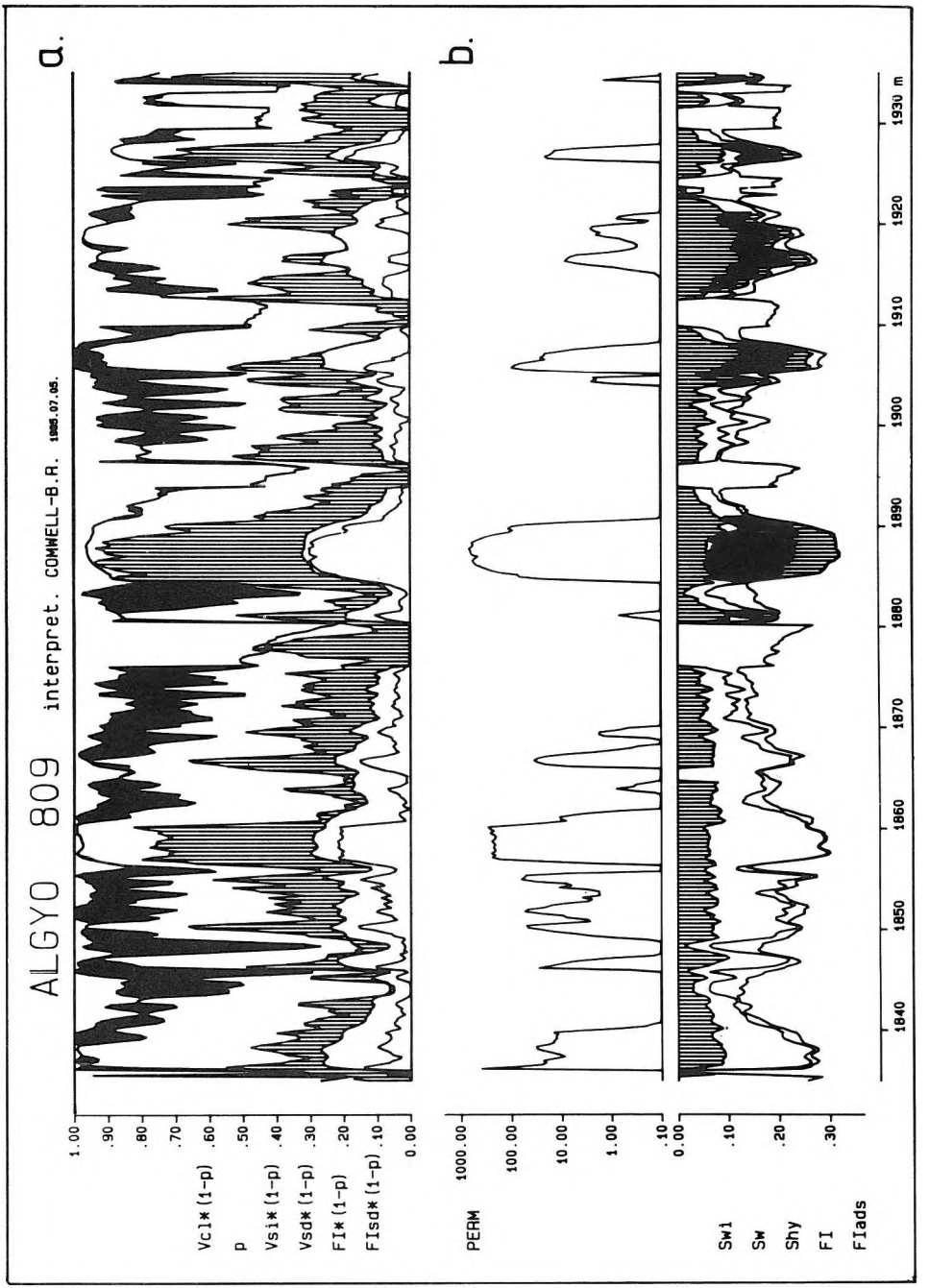
a.
ALGYO 809 interpret. COMWELL-B.R. 1985.07.05.
1.00
.90
.80
.70
Vcl*(1-p) .60
p .50
Vsi*(1-p) .40
Vsd*(1-p) .30
FI*(1-p) .20
FIsd*(1-p) .10
0.00
b.
PERM 1000.00
100.00
10.00
1.00
.10
0.00
Sw1 .10
Sw .20
Shy .30
FI
FIads
1840 1850 1860 1870 1880 1890 1900 1910 1920 1930 m

In the lowermost section of the combined plot of fluid-saturations, the adsorption porosity Φ_{ads} is shown; then the residual oil $S_{hy,r}\,\Phi$ and the moved oil $S_{hy,m}\,\Phi$ are presented. The movable water $S_{w,m}\,\Phi$ is shown without any shading; the uppermost section presents the irreducible water $S_{w,i}\,\Phi$. It is to be noted that all the fluid components have been related to the effective porosity Φ, however, the sum of Φ and Φ_{ads} results in the total porosity Φ_t of the rocks in Fig. 2/b.

Fig. 2. Well-log analysis of borehole ALGYO–809 at Algyő
a) Volumetric rock composition vs. depth $V_{cl}*(1-p)$ — clay; p — impermeable shale laminae; $V_{si}*(1-p)$ — silt; $V_{sd}*(1-p)$ — sand; $FI*(1-p)$ — effective porosity; $FI_{sd}*(1-p)$ — effective macro porosity
b) Permeability and fluid saturation vs. depth S_{wi} — irreducible water saturation; S_w — water saturation; S_{hy} — hydrocarbon saturation; FI_{ads} — porosity of adsorption water

2. ábra. Az algyői ALGYO–809 mélyfúrás vizsgálata
a) A kőzet térfogati összetétele a mélység függvényében
$V_{cl}*(1-p)$ — agyag; p — impermeábilis agyagmárga csíkok; $V_{si}*(1-p)$ — homokliszt; $V_{sd}*(1-p)$ — homok; $FI*(1-p)$ — effektív porozitás; $FI_{sd}*(1-p)$ — effektív makroporozitás
b) A permabilitás és a folyadéktelítettség a mélység függvényében
S_{wi} — redukálhatatlan víztelítettség; S_w — víztelítettség; S_{hy} — szénhidrogén telítettség; FI — effektív porozitás; FI_{ads} — adszorpciós porozitás

Рис. 2. Исследование скважины ALGYO–809 на месторождении Альдьё
а) Объемный состав пород как функция глубины $V_{cl}*(1-p)$ — глины; p — непроницаемые прослои глинистых мергелей; $V_{si}*(1-p)$ — алевриты; $V_{sd}*(1-p)$ — пески; $FI*(1-p)$ — эффективная пористость; $FI_{sd}*(1-p)$ — эффективная макропористость
b) Проницаемость и насыщенность жидкостями как функция глубины
S_{wi} — остаточная насыщенность водой; S_w — насыщенность водой; S_{hy} — насыщенность углеводородами; FI — эффективная пористость; FI_{ads} — адсорбционная пористость

REFERENCES

ALLEN D. F. 1984: Laminated sand analysis, SPWLA Trans. Paper XX

BARLAI Z. 1967: New methods for the evalutation of quantitative well logging of sandstone and shaly sandstone layers taking reference layers into consideration. VII. World Petroleum Congress Proceedings, Elsevier, Vol. 2, pp. 765–775

BARLAI Z. 1969: Well logging parameters of hydrocarbon-bearing sandstones composed of sand, silt and shale; evaluation of water saturation, porosity and grain-size distribution. SPWLA Trans. Paper X

BARLAI Z. 1972: A new theory of the well logging characteristics of hydrocarbon-bearing sandstones. SPWLA Trans. Paper J

BARLAI Z. 1974: Effects of fine grains and shale laminae on well log evaluation of the hydrocarbon-bearing Noegene sandstones in Hungary. European Symp. of SPWLA Trans. London, Paper I

BARLAI Z. 1976: Determination of permeability and specific surface area of the pore channels from well logs in fine grained sandstones. SPWLA Trans. Paper C

BARLAI Z., BERRUIN N. A., ABDEL MAWLA R. 1981: Determination of capillary displacement pressure and representative average capillary pressure vs. depth in shaly sandstones from well logs. SPWLA Trans. Paper FF

BEST D. L., GARDNER J. S., DUMANOIR J. L. 1978: A computer-processed wellsite log computation. SPWLA Trans. Paper Z

BOS M. R. E. 1982. Prolific dry oil production from sands with water saturations in excess of 50%: a study of a dual porosity system. The Log Analyst, **23,** 5, pp. 17–23

CARMAN P. C. 1956: Flow of gases through porous media. London, 182 p.

HOLTZMAN F. M. 1975: Statistical theory of the interpretation of geophysical fields. Fizika Zemli, 1, pp. 49–53

JUHÁSZ I. 1981: Normalised Q_v—the key to shaly sand evaluation using the Waxman–Smits equation in the absence of core data. SPWLA Trans. Paper Z

KOZENY J. 1927: Über die kapillare Leitung des Wassers im Boden (Aufstieg, Versickerung und Anwendung auf die Bewässerung). Sitz. Berg. Akad. Wiss. Wien, Math. Nat. (Abt. II a), Vol. 136 a, pp. 271–306

MAYER C. R., SIBBIT A. 1981: GLOBAL*, A universal logging interpretation system (in French). European Symp. of SAID Trans. Paris, Paper 5

POUPON A., CLAVIER C., DUMANOIR J., GAYMARD R., MISK A. 1970: Log analysis of sand-shale sequences—a systematic approach. JPT, **22,** July, pp. 867–881

RUHOVETS N., FERTL W. H. 1981: Digital shaly sand analysis based on Waxman–Smits model and log-derived clay-typing. European Symp. of SAID Trans. Paris, Paper 25

SALÁT P., TARCSAI GY., CSEREPES L., VERMES M., DRAHOS D. 1982: Information–statistical methods of geophysical interpretation (in Hungarian). University Textbook J 3–1311, Tankönyvkiadó, Budapest

VAJNAR E. A., KIDWELL C. M., HALEY R. A. 1977: Surprising productivity from low-resistivity sands. SPWLA Trans. Paper EE

A SZÉNHIDROGÉN-TELÍTETTSÉG, A KŐZETÖSSZETÉTEL, A POROZITÁS ÉS A PERMEABILITÁS MEGHATÁROZÁSA SZENDVICS-KIFEJLŐDÉSŰ AGYAGOS – KŐZETLISZTES HOMOKKÖVEKBEN

BARLAI Zoltán és RÉZ Ferenc

Kifejlesztettük a szénhidrogén-tároló homokkövek egy új interpretációs rendszerét: a COMWELL–B. R./ELGI rendszert, a korábban Barlai által kidolgozott elméletre alapozva. Ezt az elméletet továbbfejlesztettük és a homokköveket az alábbi 8 komponensből összetett anyagként kezeljük: 1) impermeábilis agyagmárga csíkok a szendvics-típusú homokkőben, 2) duzzadó agyagok, 3) nem duzzadó agyagok, 4) kőzetliszt, 5) homok, 6) karbonát, 7) a vékony permeábilis kőzetcsíkok effektív porozitásával jellemezhető pórusok, 8) adszorpciós vízzel töltött pórusok.

A teljes interpretációs rendszert statisztikus alapon építettük fel az ismeretlen mennyiségek túlhatározott matematikai kezelésével. Azonban a rendszer moduláris részegységekből áll, amelyeket determinisztikus interpretációs alrendszerekbe lehet összevonni. Az alrendszerek soros kalibrálást tesznek lehetővé.

Különösen érdekes lehet a szénhidrogén-telítettség értékelésének új eljárása ebben a rendszerben, mivel a szokásos eljárások gyakran kudarcot vallanak a szendvics-kifejlődésű homokkövekben. Az elméleti és gyakorlati vonatkozásokon kívül bemutatunk egy példát egy olaj- és gáztárolót harántoló fúrás értelmezésére.

ОПРЕДЕЛЕНИЕ НАСЫЩЕННОСТИ УГЛЕВОДОРОДАМИ, СОСТАВА ПОРОД И ПРОНИЦАЕМОСТИ ТОЛЩИ С ОЧЕРЕДОВАНИЕМ ГЛИНИСТО–АЛЕВРИТИСТЫХ ПЕСЧАНИКОВ

Золтан БАРЛАИ и Ференц РЕЗ

В последние годы, на базе теории, разработанной Барлаи, нами разработана новая система интерпретации песчаниковых коллекторов нефти и газа: система COMWELL–B. R./ELGI.

Указанная теория нами усовершенствована, так что песчаники рассматриваются в качестве системы из восьми компонентов: 1) непроницаемых мергельных прослоев в толщах с очередованием глинисто–алевритистых песчаников, 2) глин набухающих, 3) глин ненабухающих, 4) алевритов, 5) песков, 6) карбонатов, 7) пор, характеризуемых эффективной пористостью в маломощных прослоях проницаемых пород, 8) пор, заполненных адсорбционной водой.

Вся система интерпретации построена на статистической основе – с переоценкой неизвестных величин при математической обработке. Сама система состоит из модульных единиц, которые могут быть объединены в детерминистские интерпретационные подсистемы. Полученные подсистемы обеспечивают возможность линейной калибровки.

В данной системе особый интерес может представлять новая методика оценки насыщенности углеводородами, поскольку обычные методики часто оказываются безпомощными в случае толщ с очередованием глинисто-алевритистых песчаников. Помимо теоретических и практических аспектов представлен пример интерпретации скважины, пройденной по коллектору нефти и газа.